Suppression of Activated FOXO Transcription Factors in the Heart Prolongs Survival in a Mouse Model of Laminopathies

Gaelle Auguste, Priyatansh Gurha, Raffaella Lombardi, Cristian Coarfa, James T. Willerson, Ali J. Marian

Rationale: **Mutations in the *LMNA* gene, encoding nuclear inner membrane protein lamin A/C, cause distinct phenotypes, collectively referred to as laminopathies. Heart failure, conduction defects, and arrhythmias are the common causes of death in laminopathies.**

Objective: **The objective of this study was to identify and therapeutically target the responsible mechanism(s) for cardiac phenotype in laminopathies.**

Methods and Results: **Whole-heart RNA sequencing was performed before the onset of cardiac dysfunction in the *Lmna*$^{-/-}$ and matched control mice. Differentially expressed transcripts and their upstream regulators were identified, validated, and targeted by adeno-associated virus serotype 9-short hairpin RNA constructs. A total of 576 transcripts were upregulated and 233 were downregulated in the *Lmna*$^{-/-}$ mouse hearts ($q<0.05$). Forkhead box O (FOXO) transcription factors (TFs) were the most activated while E2 factors were the most suppressed transcriptional regulators. Transcript levels of FOXO targets were also upregulated in the isolated *Lmna*$^{-/-}$ cardiac myocytes and in the myocardium of human heart failure patients. Nuclear localization of FOXO1 and 3 was increased, whereas phosphorylated (inactive) FOXO1 and 3 levels were reduced in the *Lmna*$^{-/-}$ hearts. Gene set enrichment analysis and gene ontology showed activation of apoptosis and inflammation and suppression of cell cycle, adipogenesis, and oxidative phosphorylation in the *Lmna*$^{-/-}$ hearts. Adeno-associated virus serotype 9-short hairpin RNA–mediated suppression of FOXO TFs rescued selected molecular signatures, improved apoptosis, and prolonged survival by ≈2-fold.**

Conclusions: **FOXO TFs are activated and contribute to the pathogenesis of cardiac phenotype in laminopathies. Suppression of the FOXO TFs in cardiac myocytes partially rescues the phenotype and prolongs survival. The findings identify FOXO TFs as potential therapeutic targets for cardiac phenotype in laminopathies. (*Circ Res*. 2018;122:678-692. DOI: 10.1161/CIRCRESAHA.117.312052.)**

Key Words: forkhead transcription factors ■ gene ontology ■ genetic therapy ■ transcription factors ■ transcriptome

Heart failure is a major cause of mortality and morbidity, estimated to affect ≈6.5 million Americans ≥20 years.[1] The prevalence of heart failure, despite the remarkable progress in the management of patients with heart failure during the past 3 decades, continues to increase in part because of the aging population. Heart failure is estimated to affect ≈8 million Americans ≥18 years of age by the year 2030.[2]

Familial dilated cardiomyopathy (DCM) is a prototypic form of heart failure with reduced systolic function.[3] The genetic basis of familial DCM is partially known. *TTN* and *LMNA*, encoding the giant sarcomere protein titin and nuclear inner membrane protein lamin A/C (LMNA), respectively, are the 2 most common causal genes, accounting for ≈1/3rd of the primary DCM.[4–6] A notable feature of DCM caused by the *LMNA* mutations is a severe and progressive cardiac dysfunction, typically occurring in conjunction with conduction defects.[4,5]

Editorial, see p 646
In This Issue, see p 639
Meet the First Author, see p 640

LMNA mutations, in addition to DCM and conduction defects, cause a dozen distinct phenotypes, including Hutchinson–Gilford progeria syndrome, Emery–Dreifuss muscular dystrophy, familial partial lipodystrophy, arrhythmogenic right ventricular cardiomyopathy, restrictive dermopathy, and axonal Charcot–Marie–Tooth disease (type 2B1), which are collectively referred to as laminopathies.[7–9] The diversity of the phenotype is in accord with the ubiquitous expression of the LMNA in almost all differentiated cells, including cardiac myocytes.[10] DCM is the major cause of morbidity and mortality in laminopathies, particularly in the subset that predominantly involves the striated muscles.[4,5,11,12]

Original received September 11, 2017; revision received December 13, 2017; accepted January 05, 2018. In December 2017, the average time from submission to first decision for all original research papers submitted to *Circulation Research* was 13.60 days.

From the Center for Cardiovascular Genetics, Institute of Molecular Medicine and Department of Medicine, University of Texas Health Sciences Center at Houston (G.A., P.G., R.L., T.T.W., A.J.M.), Texas Heart Institute (J.T.W., A.J.M.); and Baylor College of Medicine, Houston, TX (C.C.).

This manuscript was sent to Roger J. Hajjar, Consulting Editor, for review by expert referees, editorial decision, and final disposition.

The online-only Data Supplement is available with this article at http://circres.ahajournals.org/lookup/suppl/doi:10.1161/CIRCRESAHA.117.312052/-/DC1.

Correspondence to Ali J. Marian, MD, Center for Cardiovascular Genetics, 6770 Bertner St, Suite C900A, Houston, TX 77030. E-mail Ali.J.Marian@uth.tmc.edu

Novelty and Significance

What Is Known?

- Mutations in *LMNA* gene cause over a dozen distinct phenotypes, including dilated cardiomyopathy.
- *LMNA* is among the common causal genes for hereditary dilated cardiomyopathy.
- The molecular pathogenesis of dilated cardiomyopathy caused by the *LMNA* mutations is largely unknown and seems to involve several signaling pathways, including MAPK (mitogen-activated protein kinase), NOTCH (neurogenic locus notch homolog protein), and canonical Wnt (wingless-related integration).
- Genetic deletion of the *Lmna* gene in mice leads to several cardiac dysfunction and premature death by 4 to 8 weeks of age.

What New Information Does This Article Contribute?

- We sequenced ribosome-depleted whole-heart transcripts (RNA sequencing) in 2-week-old *Lmna*$^{-/-}$ mice, before the onset of cardiac dysfunction, and their wild-type littermates.
- We identified ≈1000 differentially expressed genes, the majority of which were upregulated in the *Lmna*$^{-/-}$ hearts.
- Network analysis of differentially expressed genes led to identification of >2 dozen deranged upstream regulators of gene expression.
- Forkhead box O (FOXO) transcription factors were among the most activated upstream transcriptional regulators, a finding that was validated by multiple methods.
- Knockdown of FOXO1 and FOXO3 in the heart using recombinant adeno-associated viruses, expressing a sequence-specific short hairpin RNA, attenuated apoptosis and nearly doubled the survival time in the *Lmna*$^{-/-}$ mice.

The findings of the present study point to multiplicity of the pathogenic pathways dysregulated in the heart in LMNA deficiency, including activation of FOXO 1 and 3 transcription factors. The findings also identify FOXO 1 and 3 as potential therapeutic targets in dilated cardiomyopathy caused by the *LMNA* mutations. Furthermore, the findings highlight the shortcomings of targeting of a single pathogenic pathway in fully rescuing the phenotype. Therefore, targeting of multiple pathogenic pathways might be required for superior therapeutic achievements in heart failure caused by the *LMNA* mutations.

Nonstandard Abbreviations and Acronyms

AAV9	adeno-associated virus serotype 9
BW	body weight
DCM	dilated cardiomyopathy
DET	differentially expressed transcript
ETC	electron transport chain
FOXO	forkhead box O
GSEA	gene set enrichment analysis
LAD	LMNA-associated domain
LMNA	lamin A/C
PCR	polymerase chain reaction
qPCR	quantitative polymerase chain reaction
RNA-Seq	RNA sequencing
shRNA	short hairpin RNA
TF	transcription factor
WT	wild type

The molecular mechanisms leading to DCM in laminopathies are largely unknown, but expected to be diverse, in keeping with the multiple functions of LMNA in cardiac myocytes.[13,14] Alterations in signaling pathways, including MAPK (mitogen-activated protein kinase), AKT (protein kinase B), NOTCH (neurogenic locus notch homolog protein), and WNT (wingless-related integration) pathways, have been implicated along with changes in mechanotransduction and the linker of nucleoskeleton and cytoskeleton complex.[7,13,15,16] Dysregulated gene expression, proposed by Hutchinson over a decade ago,[14] has emerged as the prevailing mechanism to explain phenotypic plasticity of the *LMNA* mutations. The hypothesis is based on the known interactions of LMNA, directly or indirectly through other nuclear lamina proteins, with chromatin in >1000 genomic regions.[17–19] The LMNA-associated domains (LADs), with an average length of ≈500 kilobase pairs, are predominantly located in the heterochromatin and generally gene-poor regions, but they also involve gene-rich and the regulatory loci.[18,20–22] Consequently, LMNA is expected to influence expression of a diverse array of genes involved in various biological processes, which are likely to be pertinent to the pathogenesis of the phenotypes in laminopathies.[17,18] Thus, the purpose of the study was to identify the differentially expressed genes and their upstream (transcriptional) regulators and to determine potential beneficial effects of targeting of the main dysregulated pathway in LMNA deficiency. The objectives are to gain new insights into the molecular pathogenesis of cardiac phenotypes in laminopathies and identify new therapeutic targets.

Methods

The data, methods used in the analysis, and materials used to conduct the research will be made available to any researcher for purposes of reproducing the results or replicating the procedure. The transcriptomic data will be deposited in NCBI GEO (National Center for Biotechnology Information Gene Expression Omnibus) Profile, which will maintain the data indefinitely

A detailed Methods section has been provided as Online Data Supplement. The studies conformed to the Guide for the Care and Use of Laboratory Animals published by the US National Institutes of Health and were approved by the Animal Care and Use Committee and the Biological Safety Committee of the University of Texas Health Science Center-Houston.

Lmna$^{-/-}$ and Wild-Type (WT) Littermates

The phenotype in the *Lmna*$^{-/-}$ mice has been published.[23,24] Oligonucleotide primers used in polymerase chain reaction (PCR) reactions are listed in Online Table I.

Gross Morphology and Survival

Body weight (BW) was recorded weekly, and heart weight/BW ratio was calculated in age- and sex-matched mice. Survival was analyzed by constructing Kaplan–Meier survival plots.

Echocardiography

Cardiac size and function were assessed in age- and sex-matched mice by 2-dimensional, M mode, and Doppler echocardiography

using a Vevo 1100 ultrasound imaging system equipped with a 22- to 55-MHz MicroScan transducer (MS550D; FUJIFILM VisualSonics Inc, Toronto, ON, Canada), as published.[25–29]

Isolation of Adult Cardiac Myocytes

Adult cardiac myocytes were isolated as published.[26,29] In brief, the excised heart was perfused with a digestion buffer containing collagenase II, and the perfusion was continued until complete softening of the myocardium. The cells were dissociated from the digested hearts by gentle pipetting and were placed in a buffer containing 10% calf serum and 12.5 µmol/L $CaCl_2$ to stop the reaction. Cells were then filtered through a 100-µm nylon mesh, and myocytes were left to sediment by gravity in the presence of 2 mmol/L ATP and pelleted by centrifugation at 20*g*. Myocytes were reintroduced to calcium in stepwise concentrations of 100, 400, and 900 µm and added to the stop buffer at 2 mmol/L ATP. The isolated myocytes were resuspended in a plating media containing antibiotics, calf serum, and ATP. The isolated myocytes were placed on laminin-coated cover glasses in a 2% CO_2 incubator at 37°C or were immediately frozen.

Isolation of Neonatal Mouse Ventricular Myocytes and Transduction With Adenoviruses

Cardiac cells were isolated from 1- to 2-day old WT mice by enzymatic dispersion with collagenase and pacreatin. Neonatal mouse cardiac myocytes were separated from the rest of the cells by differential attachment and grown on chamber slides. On day 2, cells were infected with recombinant adenoviruses expressing a constitutively active form of forkhead box O (FOXO; Ad-FOXO^{AAA}) or a vector virus alone (Vector Biolabs, no. 1025 and no. 1300) for 48 hours with a multiplicity of infection of 20.[30,31] Neonatal mouse cardiac myocytes were treated for superoxide mitochondrial production detection by MitoSOX or were fixed for detection of apoptosis.

Histology

Fibrosis was assessed on staining of thin myocardial sections with Masson trichrome and Sirius Red, as described.[26,29,32] Collagen volume fraction was calculated as published.[32]

Detection of Apoptosis

Apoptosis was detected by nick-end labeling of DNA with the TUNEL (terminal deoxynucleotidyl transferase dUTP nick-end labeling) assay using In Situ Cell Death Detection Kit (Roche catalogue no. 11684795910 and 12156792910) per manufacturer instructions and quantification of the transcript levels of genes involved in apoptosis, as published.[26,29,33]

Quantitative Real-Time PCR

Total RNA was extracted from myocardial tissue or from isolated cardiac myocytes using the Qiagen miRNeasy Mini Kit (catalogue no. 217006).[25,28] Taqman probes and SYBR Green primers are detailed in Online Table I.

Immunoblotting of Total and Cellular Protein Fractions

Expression levels of the proteins of interest in mouse heart samples and isolated cardiac myocytes were detected and quantified by immunoblotting, as described.[25,26,28] Nuclear and cytosolic proteins were extracted using a commercial kit (ProteoExtract, Calbiochem, catalogue no. 539790) and probes with the specific antibodies against proteins of interest.[34] Immunofluoresences were performed on thin myocardial sections as published.[25,26,29]

RNA Sequencing

RNA sequencing was performed in the whole-heart ribosome-depleted RNA extracts from the 2-week-old WT and *Lmna*$^{-/-}$ mice on an Illumina platform, as published with minor modifications.[25,28] In brief, ribosome-depleted cardiac RNA samples were analyzed for integrity on an Agilent Bioanalyser RNA chip. Samples with high integrity index were used to prepare sequencing library using the Illumina TruSeq stranded total RNA library preparation kit. The samples were sequenced on the Illumina HiSeq 4000 instrument using the paired-end sequencing reagents to generate 100 base pair runs.

Raw RNA sequencing reads were mapped to the mouse reference genome build 10 (UCSC mm10/GRCm38) by Tophat2.[35] Gene expression was assessed using Cufflinks2 and the GENCODE gene model.[35,36] Only transcripts that exceeded 1 fragments per kilobase of transcript per million mapped fragments in at least 1 sample were included in the analyses. Differentially expressed transcripts (DETs) were identified using the edgeR analysis package in R statistical program with the significance level set at $q<0.05$ and the fold change at >1.25. Quality control and data visualization were assessed by principal components analysis and hierarchical clustering in R. GENE-E software (http://www.broadinstitute.org/cancer/software/GENE-E) was used to generate the heat maps from the raw fragments per kilobase of transcript per million mapped fragments values, and the Graph Pad Prism was used to generate the volcano plots. Enriched upstream regulators and transcription factor (TF)–binding sequence motifs were inferred using gene set enrichment analysis (GSEA; version 2.2.3, http://software.broadinstitute.org/gsea/), TF-binding motifs TRANSFAC,[37] Molecular Signature Database,[38–40] and the Ingenuity Pathway Analysis (Qiagen). Gene ontology analyses were conducted using ConsensusPathDB (release MM9-http://cpdb.molgen.mpg.de/MCPDB),[41–43] and gene ontology terms were gathered according to their similarities using REVIGO (http://revigo.irb.hr/).[44] Circos plot was generated in R using the GO-Chord option.

AAV9-Mediated In Vivo Suppression of FOXO TFs in the Heart

A previously validated short hairpin RNA (shRNA) that targets FOXO1 and FOXO3[45,46] was cloned into adeno-associated virus serotype 9 (AAV9) vectors downstream to a U6 promoter (VectoBiolab). Control AAV9 vectors contained either a GFP (green fluorescence protein) or a scrambled shRNA expression cassette. Sequence of the shRNA against FOXO1 and 3 and scrambled shRNA are presented in Online Table I.

To knockdown expression of FOXO1 and FOXO3 in the heart, recombinant AAV9 constructs at a titer of 0.5×10^{11} vector genomes per gram of BW (vg/g) were injected subcutaneously into neonatal mice, sequentially at P2, P4, and P6 postnatal days, delivering a total of 1.5×10^{11} vg/g to each mouse. Control AAV9 vectors were injected at the same dosage and time points. The early time points were chosen to allow sufficient time for gene expression before the onset of cardiac phenotypes in the *Lmna*$^{-/-}$ mice.[23,24] Serial injections before complete immune competency are expected to enhance transduction efficiency by targeting the newly formed cardiac myocytes.[47] The viral titer was chosen to induce an efficient transduction of cardiac myocytes without toxicity.[48–50]

Cytokines Measurement

Cytokine and chemokine levels in the heart of 2-week-old WT and *Lmna*$^{-/-}$ mice were measured using the Milliplex MAP Mouse Cytokine/Chemokine 32-plex assay (Millipore) according to manufacturer's protocol (MCYTMAG-70K-PX32).

Mitochondrial Electron Chain Transport Activity

Enzymatic activity of each of the complexes of mitochondrial electron transport chain (ETC) was assessed in the heart of 2-week-old WT and *Lmna*$^{-/-}$ mice by adding the specific substrates to cardiac homogenates, as published.[51] All activities were calculated as nmoles/min per milligram protein, normalized to citrate synthase activity, and expressed as a percentage of WT activity.

Mitochondrial ETC Complexes Assembly Immunoblotting

ETC complexes assembly was assessed by immunoblotting of specific subunit of each of the 5 ETC complexes using the Total OXPHOS Rodent WB Antibody Cocktail (Abcam, #ab110413) per manufacturer's instruction.

Mitochondrial Superoxide Anion Production Detection by MitoSOX

Mouse neonatal ventricular myocytes were incubated with Red MitoSOX according to manufacturer's instructions.

Statistical Analyses

Data that followed a Gaussian distribution pattern were presented as mean±SEM and were compared by *t* test and 1-way ANOVA. Otherwise, data were presented as the median values and compared by Kruskall–Wallis test, as were the categorical data. Survival rates were analyzed by constructing Kaplan–Meier survival plots and comparing the survival rate by log-rank (Mantel–Cox) test.

Results

Cardiac Phenotype in 2-Week-Old *Lmna*$^{-/-}$ Mice

To validate deletion of the *Lmna* gene, cardiac protein extracts from the WT and *Lmna*$^{-/-}$ mice were probed for the expression of the LMNA protein using an anti-LMNA antibody. As expected, expression of the LMNA protein was not detected in the heart of the *Lmna*$^{-/-}$ mice (Online Figure IA). The *Lmna*$^{-/-}$ mice survived normally within the first 2 weeks but exhibited growth retardation, as noted by the smaller BW (*Lmna*$^{-/-}$ mice: 5.44±0.2 g; WT mice: 6.97±0.3 g; $P<0.0001$; Online Figure IB and IC). Given that BW is a major determinant of cardiac size, including echocardiographic indices of left ventricular dimension, these indices were corrected for the BW. Accordingly, heart weight/BW ratio was not significantly different between *Lmna*$^{-/-}$ and WT mice (Online Figure ID). To detect early transcriptomic changes that precede cardiac dysfunction, and therefore, to reduce the confounding changes, cardiac function was analyzed in 2-week-old *Lmna*$^{-/-}$ and WT mice by echocardiography. Consistent with the previous data, there were no differences in the echocardiographic indices of cardiac size and function between 2-week-old *Lmna*$^{-/-}$ and WT mice with the exception of the mean left ventricular end-diastolic diameter corrected for BW, which was slightly enlarged in the *Lmna*$^{-/-}$ mice (by 0.05 mm/g; $P=0.032$) while left ventricular fractional shortening was normal (Online Table II).[23,24,52] Histological examinations showed no discernible cardiac fibrosis in the *Lmna*$^{-/-}$ mice at 2 weeks of age (Online Figure IE and IF). In accord with the histological findings, levels of *Col1a1*, *Col1a2*, and *Tgfb1* transcripts, markers of fibrosis, as assessed by quantitative PCR (qPCR), were unchanged in the hearts of 2-week-old *Lmna*$^{-/-}$ mice (Online Figure IG).

Differentially Expressed Cardiac Transcripts in 2-Week-Old *Lmna*$^{-/-}$ Mice

Given the absence of discernible cardiac dysfunction in the *Lmna*$^{-/-}$ mice, RNA sequencing (RNA-Seq) was performed in the ribosome-depleted cardiac transcripts isolated from the hearts of 2-week-old WT and *Lmna*$^{-/-}$ mice (whole-heart ribosome-depleted RNA). Of the 809 genes that were dysregulated in the hearts of 2-week-old *Lmna*$^{-/-}$, as compared with the WT mice, 233 were downregulated and 576 upregulated. Volcano plots and heat maps of the DETs are shown in Figure 1A and 1B.

To corroborate the DETs identified by RNA-Seq, transcript levels of randomly selected 20 dysregulated genes, showing at least a 2-fold or higher change ($q<0.05$), were analyzed by qPCR in the whole hearts in an independent set of WT and *Lmna*$^{-/-}$ mouse hearts. As shown in Figure 1C, the findings corroborated the RNA-Seq findings.

Dysregulated Upstream Transcriptional Regulators and Enriched TF-Binding Sites in the DETs in the *Lmna*$^{-/-}$ Hearts

To identify the dysregulated upstream transcriptional regulators in the *Lmna*$^{-/-}$ hearts, DETs were analyzed against the Molecular Signature Database to identify over-representation of the binding sites of the TFs in the promoter regions of the differentially expressed genes. The consensus binding motif for FOXO TFs (TTGTTT) was over-represented in the upregulated genes while the motif for E2 factors was the most over-represented in genes whose transcript levels were reduced (Figure 1D and 1E). In addition, motifs for the NFAT (nuclear factor of activated T-cells), AP1 (activator protein 1), and E12 TFs showed significant enrichment in the *Lmna*$^{-/-}$ hearts. Nevertheless, FOXO TFs had by far the most dysregulated targets (Figure 1D). Detailed results are provided in Online Table III.

Ingenuity pathway analysis of the DETs also identified FOXO3 among the top transcriptional regulators in the *Lmna*$^{-/-}$ hearts (*z* score: 3.76; $P=3.3E^{-07}$; Online Table IV). A total of 145 FOXO target genes were dysregulated in the heart of *Lmna*$^{-/-}$ mice, of which 128 were upregulated, and only 19 were downregulated (Figure 2A). The magnitude of the differential expression of FOXO TF targets is illustrated in the heat map (Figure 2B). Quantitative PCR analysis also showed increased transcript levels of *Foxo3* in the *Lmna*$^{-/-}$ mouse hearts (Figure 2C). The FOXO family of TFs share TTGTTT as their common binding site motif. Therefore, the analysis of the differentially expressed genes does not enable distinction among the specific dysregulated FOXO TFs. Therefore, network analysis by ingenuity pathway analysis showed dysregulated transcript levels of several FOXO TF targets, which were shared among the 3 common FOXO TFs expressed in the heart (Figure 2D).[53] To further corroborate activation of the FOXO TFs in the hearts in the *Lmna*$^{-/-}$ mice, transcript levels of a selected number of FOXO TF targets were analyzed by qPCR. The findings were notable for increased levels in the *Lmna*$^{-/-}$ as opposed to the WT hearts (Figure 2E).

Increased Nuclear Localization of FOXO1 and 3 in the *Lmna*$^{-/-}$ Hearts

To further corroborate evidence for the activation of FOXO TFs, levels of FOXO1, 3, and 4 transcripts and proteins were determined by qPCR, immunoblotting, and immunofluorescence, respectively. Transcript levels of *Foxo3*, the most abundant FOXO TF in the heart, but not *Foxo1* and *Foxo4*, were increased significantly in the heart, likely reflecting autoregulation (Figure 2C). Immunoblotting of myocardial nuclear protein subfraction showed increased levels of FOXO1 and FOXO3 by 1.4±0.1–fold (n=5; $P=0.035$) and 1.8±0.1–fold (n=6; $P=0.014$ versus WT), respectively, in the *Lmna*$^{-/-}$ as compared with WT mouse hearts, whereas FOXO4 levels were unchanged (Figure 3A and 3B). Levels of FOXO3 in the cytoplasmic protein fraction were unchanged while those of FOXO1 were reduced by 46.0±3.9% (n=5; $P=0.002$ versus WT; Figure 3C and 3D). Levels of FOXO1 in the total protein extracts were increased 1.6±0.2–fold (n=8–9; $P=0.0007$) while FOXO3 and FOXO4 levels were unchanged (Figure 3E and 3F). Finally, because FOXO TFs are inactivated on phosphorylation at threonine residues 24 and 32

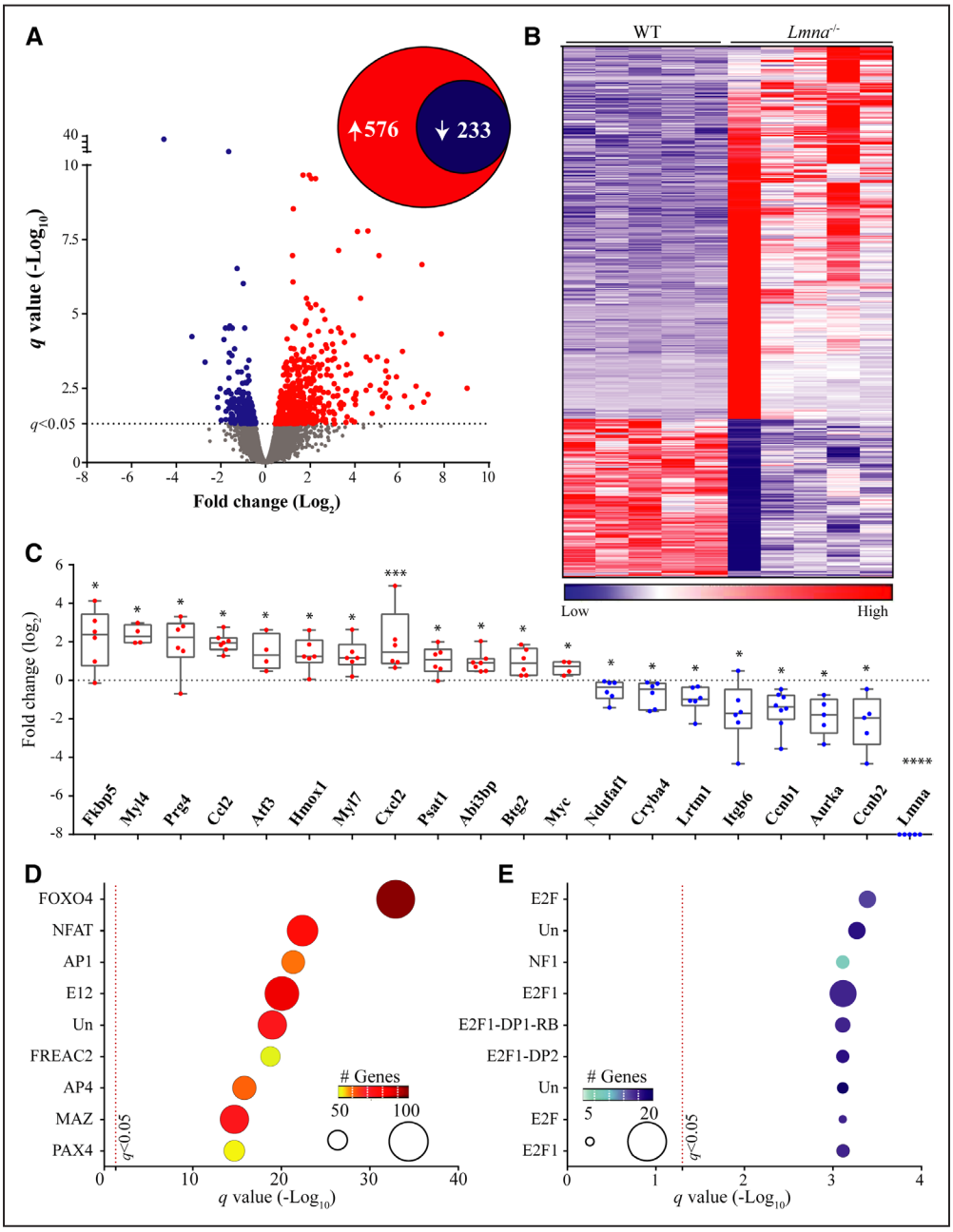

Figure 1. Cardiac RNA sequencing (RNA-Seq) data in 2-wk-old wild-type (WT) and *Lmna*$^{-/-}$ mice. A, Volcano plot of all the transcripts detected by RNA-Seq. The significance level for the differentially expressed transcripts (DETs) is marked by a dashed line at the *q* value of 0.05. A total of 809 transcripts were differentially expressed between *Lmna*$^{-/-}$ and WT, comprised 576 upregulated and 233 downregulated transcripts (insert circles). **B**, Heat map of the DETs. Transcripts were ranked, according to their differential expression across genotypes, from the most upregulated genes to the most downregulated in *Lmna*$^{-/-}$ hearts. **C**, Quantitative polymerase chain reaction validation of RNA-Seq data for 20 DETs, including *Lmna*, the latter as a control. The transcripts were randomly selected for validation among those showing ≈2-fold or higher change in RNA-Seq data and were differentially expressed at a *q* value of 0.05. Gene expression in *Lmna*$^{-/-}$ after normalization is presented here as $\log_2$ of fold change relative to the expression levels in WT mice **P*<0.05, ***P*<0.01, ****P*<0.001, *****P*<0.0001. **D** and **E**, Enrichment of conserved *cis*-regulatory motifs in DETs. DETs were analyzed using gene set enrichment analysis and the Molecular Signature Database for enrichment of transcription factor (TF)–binding motifs by hypergeometric distribution. Top 10 over-represented TFs among the upregulated (**D**) and downregulated (**E**) TFs are presented. The number of the genes in the overlap is displayed by size of the ball on the graph along with the color coding indicated in the insert. Detailed analysis is provided in Online Table III. FOXO indicates forkhead box O; and Un, unknown TF for the identified binding motif.

(Thr$^{24/32}$), pFOXO levels were determined in myocardial protein extracts using an antibody that recognizes phospho-FOXO1, 3, and 4 proteins. As shown, pFOXO1 and 3 levels were reduced by 63.4±2.6% (n=4; *P*=0.028 versus WT; Figure 3G and 3H). Consequently, the relative levels of active to inactive FOXO1 and 3 were increased in *Lmna*$^{-/-}$ as compared with control WT mouse hearts (Figure 3I). Finally, FOXO3 nuclear localization was analyzed by immunofluorescence costaining of thin myocardial sections for FOXO3 and actinin α 2, the latter as a marker for cardiac myocytes. The number of myocytes

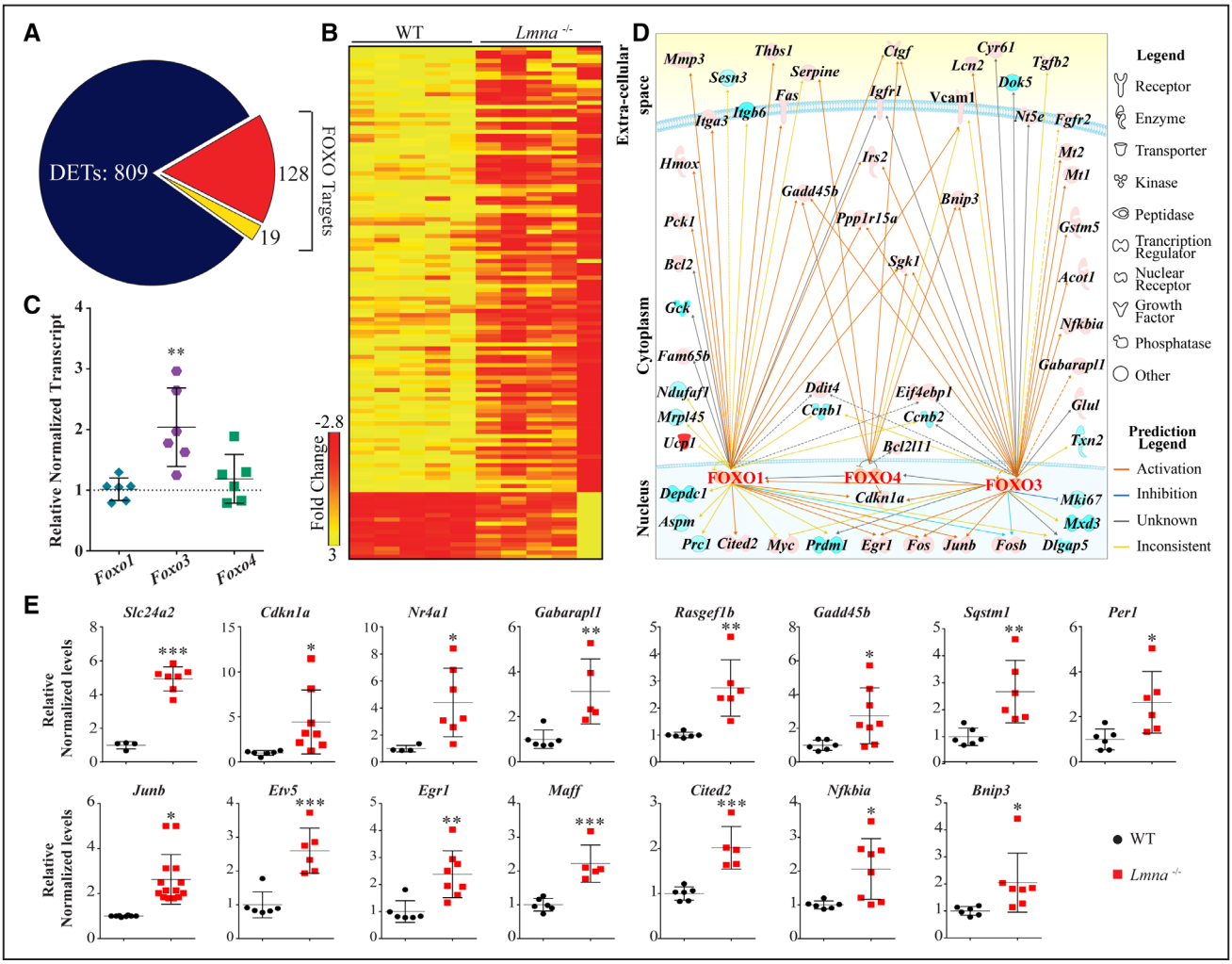

Figure 2. Activation of forkhead box O (FOXO) transcription factors (TFs) in *Lmna*$^{-/-}$ mice at 2 wk of age. A, Pie chart showing the fraction of differentially expressed transcripts (DETs) that are targets of FOXO TFs. A total of 128 targets of 809 DETs were upregulated and 19 were downregulated, as highlighted in red and yellow colors, respectively. **B**, Heat map of the DETs that are targets of the FOXO TFs shown in the wild-type (WT) and *Lmna*$^{-/-}$ mice. Heat map colors (red, upregulation; yellow, downregulation) indicate transcript fold change obtained from the RNA sequencing (RNA-Seq) data. The scale bar represents magnitude of the change. **C**, Transcript levels of *Foxo1*, *Foxo3*, and *Foxo4* in the WT and *Lmna*$^{-/-}$ mouse hearts, as quantified by quantitative polymerase chain reaction (qPCR). Among the 3 isoforms, *Foxo3* transcript levels were increased by 2.03±0.49–fold, as compared with WT mice (n=6; *P*=0.003). **D**, Upstream regulatory pathways altered in the heart in 2-wk-old *Lmna*$^{-/-}$ mice. Ingenuity Pathway Analysis (IPA) of DETs identified FOXO3 TF among the most activated pathway (*z* score: 3.75), as reflected in the increased transcript levels of >100 target genes. Interactive networks depicting increased (orange) or suppressed (blue) targets of FOXO1, 3, and 4 TFs. Solid and dashed lines represent direct and indirect interactions, respectively. The gray lines indicate predicted interactions without indication of the nature of the relationship, and the yellow interactions with opposite effects from the literature. **E**, Validation of the RNA-Seq data of FOXO TF targets by qPCR. Relative transcript levels (normalized to *Gapdh*) of over a dozen FOXO TF target genes, identified by gene set enrichment analysis and IPA analyses, in the *Lmna*$^{-/-}$ mouse hearts are depicted (n=6–8 mice per group). The findings are concordant with increased transcript levels in the RNA-Seq data.

showing localization of FOXO3 in the nucleus was increased in the *Lmna*$^{-/-}$ mouse hearts as compared with WT (1.8±0.2–fold in *Lmna*$^{-/-}$ mouse heart versus WT hearts; n=3; *P*=0.006; Figure 3J and 3K). Collectively, the findings indicate activation of FOXO1 and FOXO3 TFs in the hearts of the *Lmna*$^{-/-}$ mice.

To extend the findings on activation of FOXO TFs in the *Lmna*$^{-/-}$ mouse hearts to human hearts with DCM, publically available RNA-seq data from failing and nonfailing human hearts (GSE46224) without defined mutations were analyzed by GSEA for the TF-binding motif enrichment. As shown in Online Figure II, the TTGTTT motif was significantly enriched in the human heart samples from patients with DCM. This finding corroborates activation of the FOXO TFs in the *Lmna*$^{-/-}$ mouse hearts.

Dysregulated Biological Processes

To identify the biological processes associated with the dysregulated transcriptional regulators, cardiac transcripts were analyzed by GSEA using the Molecular Signature Database. Genes involved in inflammation, hypoxia, and apoptosis were upregulated and those involved in oxidative phosphorylation, cell cycle progression, and adipogenesis were downregulated (Figure 4A and 4B). Given that genes involved in the inflammatory responses were prominently depicted in the hearts of the *Lmna*$^{-/-}$ mice, GSEA plot and transcript levels of genes involved in the NFκB

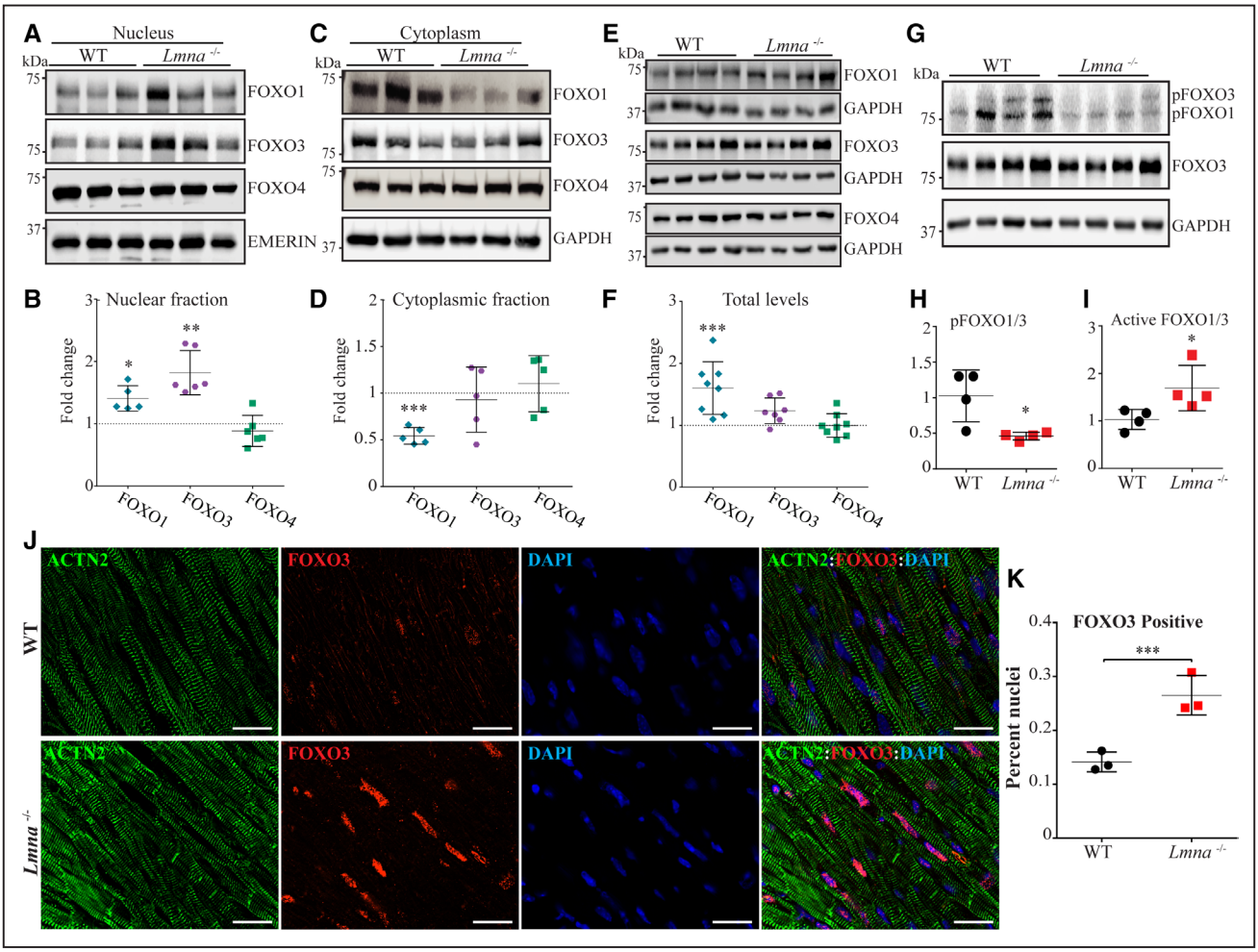

Figure 3. Increased nuclear localization of forkhead box O (FOXO) transcription factors in cardiac myocytes in the *Lmna*$^{-/-}$ mice at 2 wk of age. A and **B**, Subcellular localization of FOXO transcription factors in the heart. FOXO1, 3, and 4 proteins were detected by immunoblotting on nuclear and cytoplasmic protein fractions, as well as in the total myocardial proteins extracts from the *Lmna*$^{-/-}$ and wild-type (WT) mouse hearts (**E** and **F**). Corresponding quantitative data show increased levels of FOXO3 in the nuclear protein subfraction by 1.8±0.14–fold (**B**, n=6; *P*=0.014 vs WT). FOXO1 levels also showed a modest increase in the nuclear protein extracts in the *Lmna*$^{-/-}$ mouse heart (1.4±0.1–fold; *P*=0.035), whereas FOXO4 levels were unchanged (**B**). Level of FOXO1 in the cytoplasmic protein fraction was reduced by 46.0±3.9% (n=5; *P*=0.002 vs WT), whereas levels of FOXO3 and FOXO4 were unchanged (**C**). A modest increase in levels of FOXO1 protein in the total myocardial protein extract (1.6±0.2–fold vs WT; n=8–9; *P*=0.0007) was also noted. There were no significant differences in levels of FOXO3 and FOXO4 in the total myocardial protein extracts between the groups (**E** and **F**). **G**–**H**, Immunoblot of phospho-Thr^{24,32}-FOXO1 and 3 (pFOXO1/3), total FOXO1 and 3, and GAPDH, the latter as a loading control. Levels of pFOXO1 and 3 were reduced by 63.4±2.6% in the *Lmna*$^{-/-}$ mouse hearts (n=4; *P*=0.028 vs WT; **G** and **H**). Conversely, the estimated active to inactive FOXO1 and 3 levels (total FOXO1/3-pFOXO1/3) were increased by 2.76±0.62–fold in *Lmna*$^{-/-}$ mouse hearts (*P*=0.038 vs WT; **I**). **J** and **K**, Representative immunofluorescence staining of FOXO3 and α-actinin (ACTN2), a myocyte marker, on thin myocardial section showing increased nuclear localization of FOXO3 in cardiac myocytes in the *Lmna*$^{-/-}$ mouse hearts compared with the WT (n=3; scale bar is 20 μm; **J**). Corresponding quantitative data, based on analysis of a minimum of 21 820 nuclei per group, are shown in **K** (0.26±0.02% vs 0.14±0.01% myocytes in the *Lmna*$^{-/-}$ and WT mouse hearts, respectively; *P*=0.006). **P*<0.05, ***P*<0.01, ****P*<0.001, *****P*<0.0001.

(nuclear factor kappa-light-chain-enhancer of activated B cells) pathway were analyzed along with the protein levels of selected cytokines, the later by ELISA. GSEA plots showed marked enrichment of the NFκB pathway (Figure 4C). Likewise, mRNA levels of several NFκB target genes were increased significantly (Figure 4D). Moreover, myocardial levels of several cytokines, including CXCL1 (C-X-C motif chemokine ligand 1), CCL2 (C-C motif chemokine ligand 2), IL6 (interleukin 6), CXCL10 (C-X-C motif chemokine ligand 10), LIF (leukemia inhibitory factor), and IL9 (interleukin 9), were increased in the *Lmna*$^{-/-}$ mouse hearts as compared with WT mouse hearts (Figure 4E).

To further characterize the potential impact of FOXO activation in the heart, biological pathways that are regulated by FOXO target genes were curated using gene ontology . Gene ontology analysis of FOXO target genes identified programmed cell death as the most activated biological pathway in the *Lmna*$^{-/-}$ mouse hearts (Figure 5A). Consistent with this finding, GSEA of whole transcriptome showed enrichment of genes involved in apoptosis (Figure 5B). Transcript levels of a subset of FOXO TFs target genes involved in apoptosis were also quantified by qPCR and found to be significantly increased in the *Lmna*$^{-/-}$ mouse hearts (Figure 4C). In contrast, transcript levels of antiapoptotic gene *Bcl2* were unchanged. TUNEL assays performed on thin myocardial sections showed a 3.8±0.5–fold increase in the number of TUNEL-positive nuclei in 2-week-old *Lmna*$^{-/-}$ mouse hearts

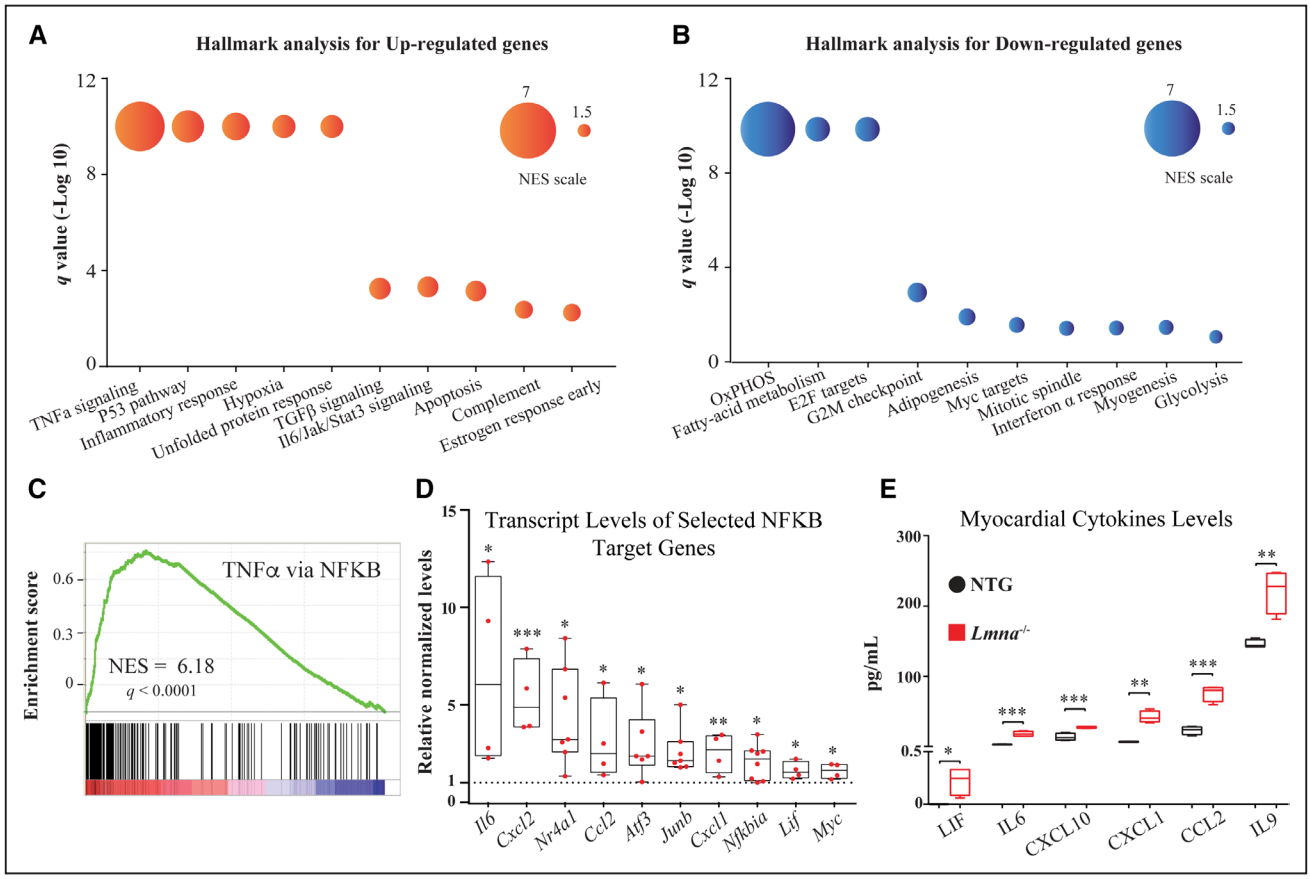

Figure 4. Dysregulated biological pathways in *Lmna*$^{-/-}$ mice at 2 wk of age. A and **B**, The list of dysregulated biological processes (upregulated in red and downregulated in blue colors) in the *Lmna*$^{-/-}$ mouse hearts (*q* value <0.05), identified by the Hallmark gene set, are shown along with circle size indicators for the normalized enrichment score (NES). **C**, Gene set enrichment analysis (GSEA) enrichment plot of TNFα (tumor necrosis factor-alpha) signaling via NFκB, the most enriched Hallmark gene set in the *Lmna*$^{-/-}$ mouse heart, showing significant enrichment of the transcript levels contributing to activation of this pathway. Distribution of the genes involved in the pathway is plotted against their individual enrichment score among the total ranked list of all transcripts analyzed by GSEA. **D**, Validation of enrichment of the TNFα signaling via NFκB in *Lmna*$^{-/-}$ mouse hearts by quantitative polymerase chain reaction for about a dozen genes involved in the pathway, showing increased transcript levels (n=4–8 per group). **E**, Levels of cytokines in the *Lmna*$^{-/-}$ mouse hearts. Levels of CXCL1 (C-X-C motif chemokine ligand 1), CCL2 (C-C motif chemokine ligand 2), IL6 (interleuikn 6), CXCL10 (C-X-C motif chemokine ligand 10), LIF (leukemia inhibitory factor), and IL9 (interleukin 9), measured by Luminex assays in the myocardial protein extracts, showing increased levels in the *Lmna*$^{-/-}$ mouse hearts as compared with wild-type (n=4 per group). **P*<0.05, ***P*<0.01, ****P*<0.001, *****P*<0.0001. NTG indicates nontransgenic.

(n=4 mice per group; *P*=0.002; Figure 5D and 5E). Finally, adenoviral-mediated expression of a constitutive active form of FOXO3 (Ad-FOXO3^{AAA}) in neonatal mouse ventricular myocytes was associated with an increased number of TUNEL-positive nuclei (3.1±0.1–fold versus control vector; *P*<0.0001; Figure 5F and 5G). Altogether, the findings indicate a deleterious role for overactivation of FOXO TFs in the hearts of the *Lmna*$^{-/-}$ mice.

Oxidative phosphorylation was the most suppressed biological function in the *Lmna*$^{-/-}$ mouse hearts (Figure 4B). Its suppression was demonstrated by GSEA, quantification of the transcript levels of selected mitochondrial genes, and determination of mitochondrial ETC activity (Online Figure III). Complex I enzymatic activity was decreased by 37.0±7.8% (n=4; *P*=0.021 versus WT) and the transcript levels of the corresponding genes involved in complex I were also reduced (Online Figure III). Likewise, suppression of the cell cycle regulatory pathways, namely E2 factor targets and G2M checkpoint, were confirmed in the *Lmna*$^{-/-}$ mouse hearts by GSEA along with quantification of transcript levels of selected genes in the pathways (Online Figure III).

Suppression of FOXO TFs in the *Lmna*$^{-/-}$ Hearts

To establish the pathogenic role of activation of FOXO TFs in cardiac phenotypes in the *Lmna*$^{-/-}$ mice, recombinant AAV9 constructs were generated to target FOXO1 and 3 on expression of an established sequence-specific shRNA (AAV9-*Foxo*^{shRNA}).[45,46] A prelude to AAV9-mediated gene targeting, which predominantly transduces cardiac myocytes,[54,55] is evidence of activation of FOXO TFs in cardiac myocytes. Accordingly, cardiac myocytes were isolated from the WT and *Lmna*$^{-/-}$ mouse hearts and analyzed for the transcript levels of 15 randomly selected FOXO TF targets by qPCR. The results (Figure 6A) showed increased transcript levels of FOXO TF target genes in cardiac myocytes isolated from the *Lmna*$^{-/-}$ mouse hearts, indicating activation of the FOXO TFs in the *Lmna*$^{-/-}$ cardiac myocytes.

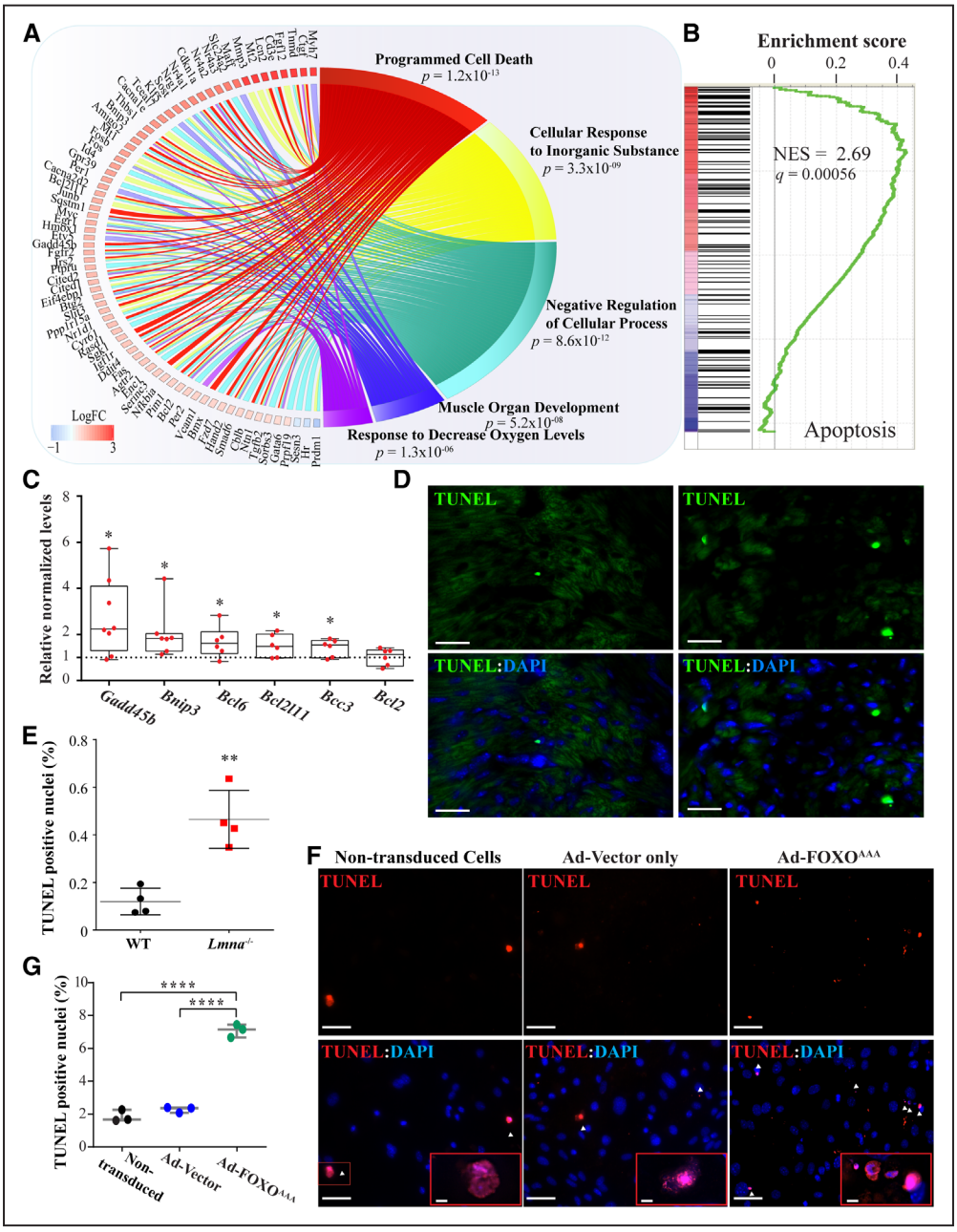

Figure 5. Activated biological pathways in the *Lmna*$^{-/-}$ mouse hearts. A, Circos plot depicting the top 5 enriched biological pathways associated with the differentially expressed forkhead box O (FOXO) transcription factor target genes, as identified by gene ontology (GO) analysis and then compiled by relative similarity using Revigo. Expression level of genes involved in the pathway is indicated in log2 of fold change. As shown, programmed cell death (apoptosis) was the most dysregulated biological process. **B**, Gene set enrichment analysis plot showing enrichment of genes involved in apoptosis. **C**, Quantitative real-time polymerase chain reaction showing increased transcript levels of selected genes involved in the apoptosis process. **D** and **E**, Apoptosis staining by TUNEL (terminal deoxynucleotidyl transferase dUTP nick-end labeling) labeling of thin myocardial sections and the corresponding quantitative data showing increased number of TUNEL (green)-positive DAPI (4',6-diamidino-2-phenylindole)-stained nuclei (blue) in the *Lmna*$^{-/-}$ mouse hearts by 3.8±0.5–fold (n=4; *P*=0.002 vs wild type). Scale bar is 10 μm. **F** and **G**, TUNEL assay of mouse neonatal ventricular myocytes (mNVM) after infection with adenoviruses expressing a constitutively active form of FOXO3 (Ad-FOXO3^{AAA}) and corresponding quantitative data showing an increased number of TUNEL (red)-positive DAPI-stained nuclei (blue) compared with control adenovirus (n=3; 3.1±0.1–fold; *P*<0.0001) or cell not infected (n=3; 3.8±0.1–fold; *P*<0.0001). No significant changes in the number of TUNEL-positive nuclei between the mNVM infected with the control adenovirus and the cells not infected (2.3±0.1% vs 1.8±0.2%; *P*=0.3). Scale bar is 50 and 5 μm in the insert.

Recombinant AAV9-*Foxo*^{shRNA}, AAV9-*Gfp*, or AAV9-scrambled^{shRNA} were injected at P2, P4, and P6 days at a total 1.5×10^{11} vg/g particles subcutaneously, followed by testing for knockdown of FOXO1 and FOXO3 TF at 2 weeks and phenotypic characterization at 4 weeks of age (Figure 6B). Treatment with the control AAV9 constructs (AAV9-*Gfp* and AAV9-scrambled^{shRNA}) had no discernible effect on the survival rate (Online Figure IV). Therefore, in the subsequent studies, AAV9-scrambled^{shRNA} construct was used as a control group. Administration of AAV9-*Foxo*^{shRNA} reduced

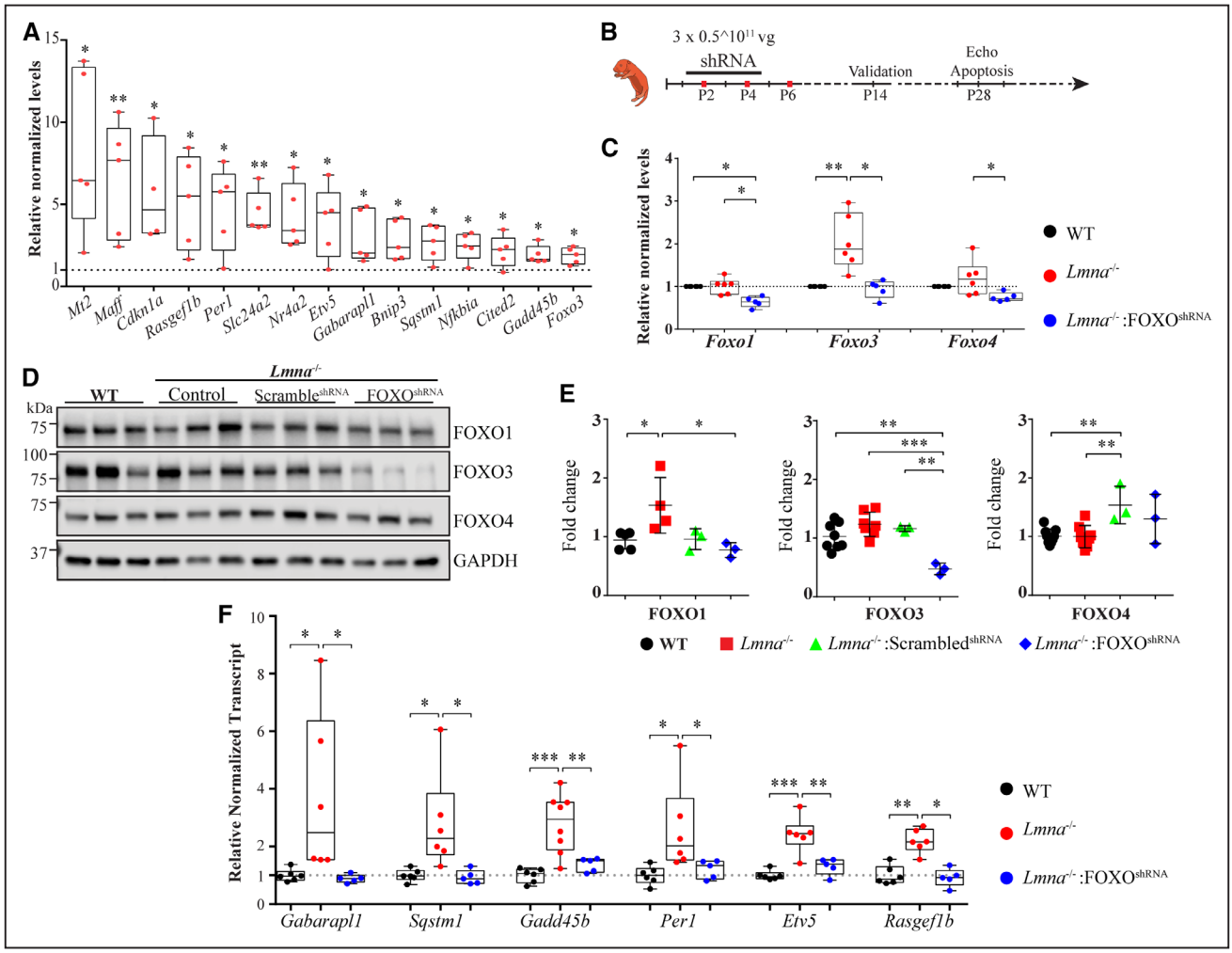

Figure 6. Knockdown of forkhead box O (FOXO) transcription factors (TFs) in *Lmna*$^{-/-}$ mouse heart. **A**, Validation of FOXO TFs activation in cardiac myocytes isolated from the *Lmna*$^{-/-}$ mouse hearts. Transcript levels of 15 FOXO TFs target genes were quantified by real-time quantitative polymerase chain reaction (RT-qPCR) on mRNA extracted from isolated cardiac myocytes from the wild-type (WT) and *Lmna*$^{-/-}$ mice. As shown, transcript levels were significantly increased in isolated cardiac myocytes form the *Lmna*$^{-/-}$ mice (n=4–5 independent myocyte isolations per group). **B**, Schematic presentation of the gene therapy protocol to knockdown FOXO TFs on injection of the recombinant adeno-associated virus serotype 9 (AAV9) constructs. Recombinant AAV9-*Foxo*^{shRNA} viral vectors were injected sequentially at postnatal day 2, 4, and 6 (P2, P4, and P6) subcutaneously at 0.5×10^{11} viral genomes (vg) per gram. Knockdown of FOXO TF was confirmed in 2-wk-old mice, and phenotypic characterization was performed at 4 wk of age. **C**, Validation of FOXO TFs knock-down at the mRNA level in the *Lmna*$^{-/-}$ mouse hearts. Transcript levels of *Foxo1*, *3*, and *4* were quantified by RT-qPCR on whole-heart mRNA extracts from the WT and *Lmna*$^{-/-}$ and *Lmna*$^{-/-}$ mice injected with the recombinant AAV9 vectors. *Foxo1* mRNA levels were decreased by 36.25±5.57% in the AAV9-*Foxo*^{shRNA} as compared with control (not injected) *Lmna*$^{-/-}$ mice (P=0.018) and to 36.3±12% compared with the WT mice (n=5–6 per group; P=0.022). *Foxo3* mRNA level was decreased to 53.7±10% in the AAV9-*Foxo*^{shRNA}-treated mice compared with nontreated *Lmna*$^{-/-}$ (P=0.026). *Foxo4* levels are reduced by 37.4±18% in the AAV9-treated mice compared with *Lmna*$^{-/-}$ (uninjected) mice (n=5–6 mice per group; P=0.024) and were unchanged compared with WT mice. **D** and **E**, Knockdown of FOXO proteins in *Lmna*$^{-/-}$ mouse hearts. **D**, Immunoblots of FOXO1, 3, and 4 proteins in protein extracted from whole heart in the experimental groups. Quantitative data for FOXO1, 3, and 4 protein levels are depicted in **E**. GAPDH was used as loading control. **F**, Normalization of FOXO TFs target transcript levels on administration of the recombinant AAV9-*Foxo*^{shRNA} construct to the *Lmna*$^{-/-}$ mice. Transcript levels of selected FOXO TF target genes were quantified by RT-qPCR in cardiac mRNA extracts from the WT and *Lmna*$^{-/-}$ (untreated) and *Lmna*$^{-/-}$ mice treated with AAV9-*Foxo*^{shRNA}. As shown, injection of AAV9-*Foxo*^{shRNA} normalized increased transcript levels of the FOXO TF target genes. *P<0.05, **P<0.01, ***P<0.001, ****P<0.0001. shRNA indicates short hairpin RNA.

Foxo3 transcript levels by 53.7±10% (P=0.026 compared with noninjected *Lmna*$^{-/-}$ mouse heart), which were increased in the *Lmna*$^{-/-}$ mouse hearts, effectively normalizing the levels (comparable to WT). Likewise, transcript levels of *Foxo1* and *Foxo4* were reduced significantly in the AAV9-*Foxo*^{shRNA} group as compared with noninjected *Lmna*$^{-/-}$ mice (37.8±12%, P=0.017, and 37.4±18%, P=0.024, respectively, Figure 6C). At the protein level, the most remarkable finding was reduced levels of FOXO3 on delivery of AAV9-*Foxo*^{shRNA} construct, which was reduced by 61.6±4.5% compared with noninjected *Lmna*$^{-/-}$ mice (n=3; P=0.024; Figure 6D and 6E). Likewise, levels of FOXO1 protein were also reduced (49.5±13.9%; P=0.006 versus noninjected *Lmna*$^{-/-}$ mice) and were comparable to those in the WT mice while levels of FOXO4 were unchanged (Figure 6D and 6E). To further support effective knockdown of FOXO TF activities on administration of the AAV9-*Foxo*^{shRNA} construct, transcript levels of several well-established FOXO TFs targets were quantified by qPCR. The

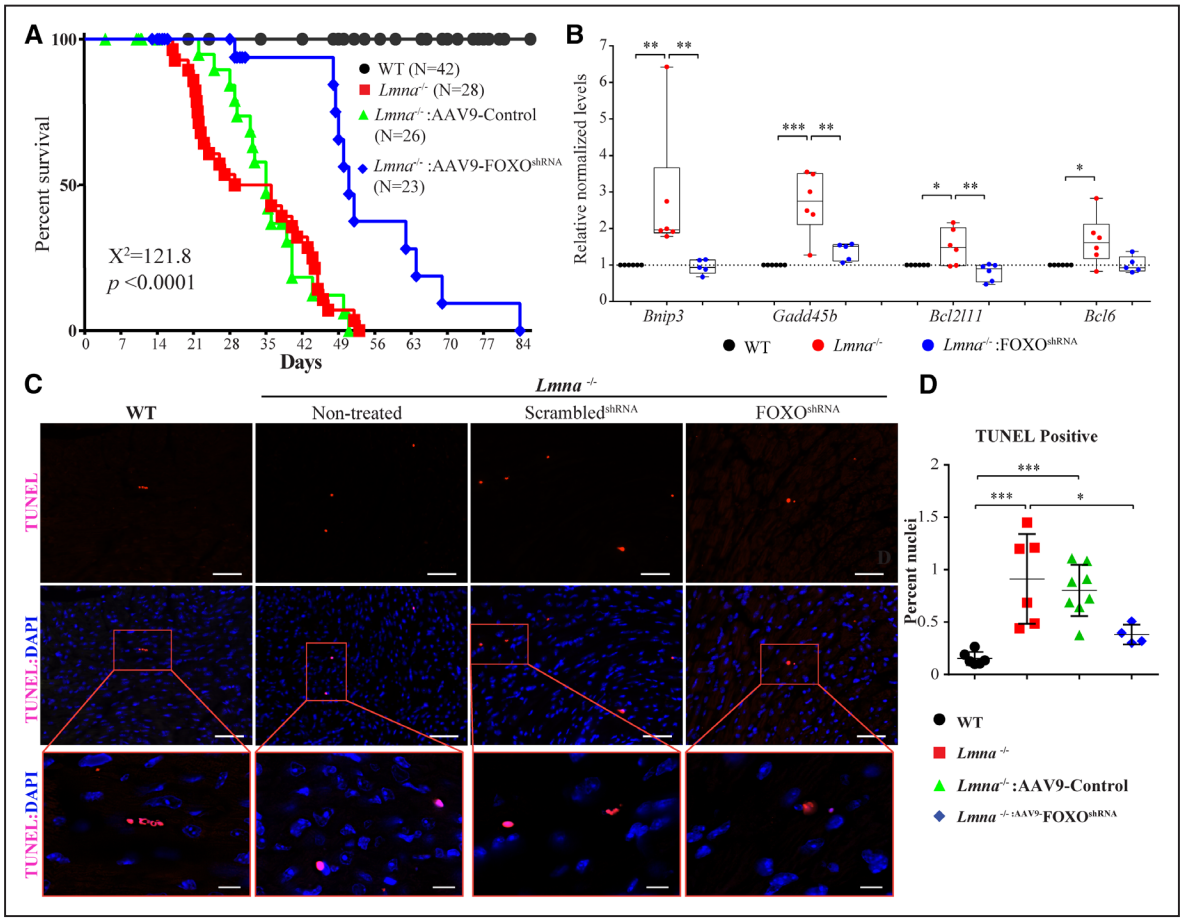

Figure 7. Phenotypic consequences of knockdown of forkhead box O (FOXO) transcription factors (TFs) in the *Lmna*$^{-/-}$ mouse hearts. A, Kaplan–Meier survival plots of wild-type (WT), *Lmna*$^{-/-}$ mice (not injected), *Lmna*$^{-/-}$ mice injected with adeno-associated virus serotype 9 (AAV9)-scrambled^{shRNA}, or AAV9-control (combined AAV9-scrambled^{shRNA} and AAV9-*Gfp*) and *Lmna*$^{-/-}$ mice injected with the AAV9-*Foxo*^{shRNA} constructs. The median survival time of *Lmna*$^{-/-}$ mice was increased from 29 to 51 d on administration of the AAV9-*Foxo*^{shRNA} construct. The survival rates in the *Lmna*$^{-/-}$ mice injected with AAV9-*Gfp* or AAV9-scrambled^{shRNA} constructs were similar to that in the (noninjected) *Lmna*$^{-/-}$ mice and are shown individually in Online Figure V. **B**, Transcript levels of selected markers of apoptosis, which are known to be FOXO TF targets, in the experimental groups. Transcript levels of BCL2-interacting protein 3 (*Bnip3*), growth arrest and DNA damage inducible β (*Gadd45b*), BCL2-like 11 (*Bcl2l11*), and B-cell CLL/Lymphoma 6 (*Bcl6*), quantified by real-time quantitative polymerase chain reaction from mRNA extracted from 2-wk-old WT, *Lmna*$^{-/-}$ mice (not injected), and *Lmna*$^{-/-}$ mice injected with the AAV9-*Foxo*^{shRNA} construct, were normalized in the treated group. **C**, Apoptosis assessments by TUNEL (terminal deoxynucleotidyl transferase dUTP nick-end labeling) assay in the heart at 4 wk of age. Representative TUNEL-stained thin myocardial cross-section from 4-wk-old WT, *Lmna*$^{-/-}$ mice (not injected), and *Lmna*$^{-/-}$ mice injected either with AAV9-scrambled^{shRNA} or the AAV9-*Foxo*^{shRNA} constructs are shown. **Top**, TUNEL staining in red. **Middle**, Overlay of TUNEL (red) and DAPI (4',6-diamidino-2-phenylindole)-stained nuclei (blue) myocardial sections. **Bottom**, Magnification of selected areas displaying apoptotic cells. Bar is 50 μm in **top** and **middle** and 20 μm in the **bottom**. Quantitative data of the TUNEL-positive stained nuclei in the experimental groups are shown in **D**. The number of apoptotic cells was increased by 5.9±1.13–fold in *Lmna*$^{-/-}$ mice (*P*=0.0008 vs WT); whereas the number in the AAV9-*Foxo*^{shRNA}-treated group was reduced by 58.2±5.1% (*P*=0.0247) compared with the nontreated *Lmna*$^{-/-}$ mice and tend to be decreased (*P*=0.071) compared with treated *Lmna*$^{-/-}$ mice. The number of apoptotic cells in the AAV9-*Foxo*^{shRNA} treated *Lmna*$^{-/-}$ mice was not significantly different from that in the WT mice (0.38±0.05% vs 0.15±0.02%, respectively; *P*=0.55). **P*<0.05, ***P*<0.01, ****P*<0.001, *****P*<0.0001. Gfp indicates green fluorescence protein; and shRNA, short hairpin RNA.

results are remarkable for normalization of the transcript levels of FOXO TF targets in AAV9-*Foxo*^{shRNA} group (Figure 6F).

Partial Phenotypic Rescue on Knockdown of FOXO TFs

To determine whether knockdown of FOXO TFs rescues the phenotype in the *Lmna*$^{-/-}$ mice, the effects of administration of the AAV9-*Foxo*^{shRNA} construct on survival, cardiac function, and apoptosis were analyzed. Knockdown of FOXO TFs in the heart was associated with ≈2-fold prolongation of survival in the *Lmna*$^{-/-}$ mice as compared with untreated *Lmna*$^{-/-}$ mice or *Lmna*$^{-/-}$ mice injected with the control AAV9-*Gfp* or AAV9-scrambled^{shRNA} vector constructs (Figure 7A; Online Figure IV). Accordingly, the median survival time was increased from 29 days in the untreated *Lmna*$^{-/-}$ mice to 52 days in the AAV9-*Foxo*^{shRNA}–treated mice.

Given marked activation of the apoptotic pathways in the *Lmna*$^{-/-}$ mouse hearts, effects of knockdown of FOXO TFs on myocardial apoptosis were analyzed. Treatment with the AAV9-*Foxo*^{shRNA} was associated with normalization of transcript levels of several genes involved in apoptosis, which are known to be FOXO TF targets (Figure 7B). Consistent with this finding, knockdown of FOXO TFs in the heart was associated with a significant reduction in

the number of TUNEL-positive cells in the myocardium (58.2±18.6%; P=0.025 versus noninjected *Lmna*$^{-/-}$ mice; Figure 7C and 7D).

Administration of AAV9-*Foxo*^{shRNA} did not have a significant effect on cardiac function (Online Table VI). However, because of the presence of significant differences in the BW between the WT and *Lmna*$^{-/-}$ mice and BW dependence of the left ventricular dimensions, the effects on cardiac functions could not be reliably assessed. To determine whether knockdown of FOXO TFs had an effect on mitochondrial functions, selected parameters of mitochondrial functions were determined in the experimental groups (Online Figure V). Integrity of the mitochondrial ETC complexes is reflected by the stable levels of known constituents of each complex, such as NDUFB8 for complex I and ATP5A for complex V. Therefore, levels of these labile protein constituents of mitochondrial ETC were quantified by immunblotting. As shown, only levels of NDUFB8 were reduced in the *Lmna*$^{-/-}$ mice (Online Figure V). Administration of AAV9-FOXO^{shRNA} did not rescue reduced levels of NDUFB8 and had no effect on other labile protein constituents of ETC, indicating a mechanism independent of FOXO TFs (Online Figure V). Likewise, MitoSOX assay showed no significant effect on superoxide production in the neonatal mouse cardiac myocyte transduced with recombinant adenoviruses expressing constitutively active FOXO TFs (Online Figure V). Moreover, no significant differences in the percent collagen volume fraction, indicative of interstitial fibrosis, were noted among the experimental groups (Online Figure VI). Finally, myocardial architectures, as assessed by staining for actinin α 2 and JPH2 (junctophilin 2), were not affected in the *Lmna*$^{-/-}$ mice treated with adenoviral vector alone and after knockdown of FOXO TFs in the heart (Online Figure VII).

Discussion

We identified ≈800 DETs in the hearts of *Lmna*$^{-/-}$ mice, which occurred in the absence of and before the onset of cardiac dysfunction. Dysregulated gene expression is in accord with the known role of LMNA in influencing chromatin structure through the LADs and regulation of gene expression.[17,18,20,21] Most of the dysregulated transcripts were upregulated, which is consistent with the data suggesting that most genes at the LADs are transcriptionally silent or suppressed.[17,19,20] Because the changes occurred in the absence of and preceded discernible cardiac dysfunction, they are likely pathogenic and partly responsible for the cardiac phenotype, as opposed to being secondary to cardiac dysfunction. Bioinformatics analyses complemented with biological validations identified FOXO TFs as among the most activated transcriptional regulators in LMNA-deficient hearts. Knockdown of FOXO1 and FOXO3 using recombinant AAV9 expressing an established anti-FOXO1 and 3 shRNA indicated a pathogenic role for the FOXO TFs in induction of apoptosis and increased mortality in the *Lmna*$^{-/-}$ mice. Overall, these findings implicate FOXO TFs as an important transcriptional regulator in the pathogenesis of the cardiac phenotypes in laminopathies.

RNA-Seq was performed on ribosome-depleted whole-heart transcriptomes. Given the ubiquitous expression of LMNA in multiple cardiac cell types, DETs are expected to originate from multiple cell types. Likewise, cardiac phenotypes in laminopathies are expected to arise from pathogenic involvement of multiple cell types. In the present study, upregulation of FOXO TF targets were verified in the heart as well as in cardiac myocytes isolated from the *Lmna*$^{-/-}$ mouse hearts. In addition, partial rescue of cardiac phenotype on knockdown of FOXO TFs using recombinant AAV9, which predominantly target cardiac myocytes in the heart,[54,55] signifies the biological effects of activation of FOXO TFs in cardiac myocytes in lamin deficiency. Moreover, doubling of survival and marked reduction in apoptosis on targeting of FOXO TFs in cardiac myocytes emphasize the biological significance of this regulatory network in cardiac myocytes in laminopathies. The findings also point to the complexity of pathways involved in the pathogenesis of cardiac phenotypes in laminopathies. Hence, targeting of multiple pathways is expected to be required for therapeutic and preventive gains in this complex disorder.

Several measures were built into the study design to identify the primary transcriptomic changes and reduce the chance of fortuitous findings and the confounding factors. Transcriptomic changes were defined before and in the absence of discernible cardiac dysfunction, which enabled identification of dysregulated pathogenic pathways in the heart in laminopathies. Likewise, reversal of these molecular events along with partial phenotypic rescue supports the pathogenic role of FOXO TFs in induction of cardiac phenotype in laminopathies. To reduce the possibility of fortuitous effects, 2 control viral vectors, one expressing a scrambled shRNA and the other expressing the GFP protein but not an shRNA, were included as controls. To increase the transduction efficiency and hence garner robust data, recombinant AAV9 vectors were delivered in 3 sequential injections, with the last injection at P6. This approach is expected to transduce the newly formed cardiac myocytes, which occurs in the early postnatal days.[47] In addition, sequential injections during the early postnatal days was designed to avoid potential neutralizing effects of the antibodies against AAV9 capsids. Overall, the design of the study enabled garnering less confounded data.

The study has several shortcomings. The mechanism(s) responsible for doubling of the survival on knockdown of FOXO TFs is unclear. Whereas the number of apoptotic cells in the myocardium was significantly reduced, cardiac function, as assessed by echocardiography, was not improved. The presence of significant differences in BWs, major determinants of echocardiographic indices of cardiac size and function, among the experimental groups, hindered robust conclusions on the effects on cardiac function. In addition to heart failure, cardiac arrhythmias are also important causes of death in patients with laminopathies.[4,5] Telemetric cardiac rhythm monitoring and electrophysiological studies were not performed in these mice, partly because of the small size of the *Lmna*$^{-/-}$ mice, to determine contributions of cardiac arrhythmias to premature death and improved survival in the experimental groups. It is also noteworthy that AAV9 constructs, despite their well-established tropism for cardiac myocytes,[54,55] also transduce skeletal muscles, including the

diaphragm, and to a lesser extent the liver.[56,57] Consequently, the survival benefit observed in the *Lmna*$^{-/-}$ mice on administration of AAV9-*Foxo*^{shRNA} might be because of the effects of suppression of FOXO TF in other organs, such as the striated respiratory muscles, prevention of muscle atrophy, and the resultant improvement in respiratory efficiency, as shown in other models.[58,59]

The observed beneficial effects of suppression of FOXO TFs on survival and apoptosis are in agreement with the previous data showing deleterious effects of activation of FOXO3 in the heart but in apparent discord with its cardioprotective role, reported in the knock out studies.[60,61] The key distinction, as opposed to the knock out studies, is that FOXO TFs were only partially suppressed and not totally abolished in our studies. Although excessive suppression, such as in genetic knock out studies, as well as excessive overexpression of FOXO TFs in the heart are expected to be deleterious, partial suppression of the already activated FOXO TFs is likely to beneficial.[62]

The mechanistic basis of DETs and activation of FOXO TFs in the heart is unclear. Whether changes in the transcriptomics are the direct consequences of dysregulated LADs resulting from the deficiency of LMNA or are the consequences of impaired assembly of the other chromatin components to the LADs remain to be determined. Likewise, specific LADs in cardiac myocytes that are dysregulated in the absence of LMNA have yet-to-be identified. Therefore, direct data to show enrichment of LMNA and likewise, enrichment of the FOXO TFs on the promoter regions of their targets could not be demonstrated because of an inadequate quality of the available anti-LMNA and anti-FOXO antibodies for chromatin immunoprecipitation studies. Nevertheless, activation of FOXO1 and FOXO3 was confirmed at multiple levels, including their nuclear localization and reduced FOXO3 phosphorylation, as well as increased transcript levels of its target genes. Moreover, specific targeting of FOXO TFs by an shRNA, whose effectiveness has been shown in independent studies,[45,46] in cardiac myocytes using AAV9 constructs partially rescued the molecular (gene expression), biological (apoptosis), and clinical (mortality) phenotypes. Collectively, these findings lend further support to the pathogenic activation of FOXO TFs in induction of cardiac phenotypes in laminopathies.

Analysis of RNA-Seq data shows activation of FOXO TFs in human heart failure with undefined mutations. Although preliminary and requiring testing for replication in additional samples and validation by complementary techniques, activation of FOXO TFs might be a general feature of heart failure and not specific to laminopathies. Consequently, one might speculate that FOXO TFs might be therapeutic targets in garden variety form of heart failure.

In conclusion, the findings implicate LMNA in the transcriptional regulation of several hundred genes and over a dozen upstream transcriptional regulators, including FOXO TFs in the heart. Dysregulations of these networks of TFs collectively, and FOXO1 and FOXO3 particularly, are in part responsible for induction of cardiac phenotype and early mortality in laminopathies. The findings identify FOXO TFs as potential targets to prevent or attenuate cardiac phenotype in laminopathies.

Sources of Funding

This work was supported, in part, by grants from National Institutes of Health (NIH), National Heart, Lung and Blood Institute (R01 HL088498 and 1R01HL132401), Leducq Foundation (14 CVD 03), George and Mary Josephine Hamman Foundation, and American Heart Association Beginning Grant in Aid (15BGIA25080008 to R. Lombardi).

Disclosures

None.

References

1. Benjamin EJ, Blaha MJ, Chiuve SE, et al; American Heart Association Statistics Committee and Stroke Statistics Subcommittee. Heart disease and stroke statistics-2017 update: a report from the American Heart Association. *Circulation*. 2017;135:e146–e603. doi: 10.1161/CIR.0000000000000485.
2. Heidenreich PA, Albert NM, Allen LA, Bluemke DA, Butler J, Fonarow GC, Ikonomidis JS, Khavjou O, Konstam MA, Maddox TM, Nichol G, Pham M, Piña IL, Trogdon JG; American Heart Association Advocacy Coordinating Committee; Council on Arteriosclerosis, Thrombosis and Vascular Biology; Council on Cardiovascular Radiology and Intervention; Council on Clinical Cardiology; Council on Epidemiology and Prevention; Stroke Council. Forecasting the impact of heart failure in the United States: a policy statement from the American Heart Association. *Circ Heart Fail*. 2013;6:606–619. doi: 10.1161/HHF.0b013e318291329a.
3. McNally EM, Mestroni L. Dilated cardiomyopathy: genetic determinants and mechanisms *Circ Res*. 2017;121:731–748.
4. Fatkin D, MacRae C, Sasaki T, et al. Missense mutations in the rod domain of the lamin A/C gene as causes of dilated cardiomyopathy and conduction-system disease. *N Engl J Med*. 1999;341:1715–1724. doi: 10.1056/NEJM199912023412302.
5. Taylor MR, Fain PR, Sinagra G, et al; Familial Dilated Cardiomyopathy Registry Research Group. Natural history of dilated cardiomyopathy due to lamin A/C gene mutations. *J Am Coll Cardiol*. 2003;41:771–780.
6. Herman DS, Lam L, Taylor MR, et al. Truncations of titin causing dilated cardiomyopathy. *N Engl J Med*. 2012;366:619–628. doi: 10.1056/NEJMoa1110186.
7. Schreiber KH, Kennedy BK. When lamins go bad: nuclear structure and disease. *Cell*. 2013;152:1365–1375. doi: 10.1016/j.cell.2013.02.015.
8. Quarta G, Syrris P, Ashworth M, Jenkins S, Zuborne Alapi K, Morgan J, Muir A, Pantazis A, McKenna WJ, Elliott PM. Mutations in the lamin A/C gene mimic arrhythmogenic right ventricular cardiomyopathy. *Eur Heart J*. 2012;33:1128–1136. doi: 10.1093/eurheartj/ehr451.
9. Liang JJ, Grogan M, Ackerman MJ. LMNA-mediated arrhythmogenic right ventricular cardiomyopathy and Charcot-Marie-Tooth type 2B1: a patient-discovered unifying diagnosis. *J Cardiovasc Electrophysiol*. 2016;27:868–871. doi: 10.1111/jce.12984.
10. Röber RA, Weber K, Osborn M. Differential timing of nuclear lamin A/C expression in the various organs of the mouse embryo and the young animal: a developmental study. *Development*. 1989;105:365–378.
11. Anselme F, Moubarak G, Savouré A, Godin B, Borz B, Drouin-Garraud V, Gay A. Implantable cardioverter-defibrillators in lamin A/C mutation carriers with cardiac conduction disorders. *Heart Rhythm*. 2013;10:1492–1498. doi: 10.1016/j.hrthm.2013.06.020.
12. van Berlo JH, de Voogt WG, van der Kooi AJ, van Tintelen JP, Bonne G, Yaou RB, Duboc D, Rossenbacker T, Heidbüchel H, de Visser M, Crijns HJ, Pinto YM. Meta-analysis of clinical characteristics of 299 carriers of LMNA gene mutations: do lamin A/C mutations portend a high risk of sudden death? *J Mol Med (Berl)*. 2005;83:79–83. doi: 10.1007/s00109-004-0589-1.
13. Carmosino M, Torretta S, Procino G, Gerbino A, Forleo C, Favale S, Svelto M. Role of nuclear lamin A/C in cardiomyocyte functions. *Biol Cell*. 2014;106:346–358. doi: 10.1111/boc.201400033.
14. Hutchison CJ. Lamins: building blocks or regulators of gene expression? *Nat Rev Mol Cell Biol*. 2002;3:848–858. doi: 10.1038/nrm950.
15. Stroud MJ, Banerjee I, Veevers J, Chen J. Linker of nucleoskeleton and cytoskeleton complex proteins in cardiac structure, function, and disease. *Circ Res*. 2014;114:538–548. doi: 10.1161/CIRCRESAHA.114.301236.
16. Brayson D, Shanahan CM. Current insights into LMNA cardiomyopathies: existing models and missing LINCs. *Nucleus*. 2017;8:17–33. doi: 10.1080/19491034.2016.1260798.

17. Paulsen J, Sekelja M, Oldenburg AR, Barateau A, Briand N, Delbarre E, Shah A, Sørensen AL, Vigouroux C, Buendia B, Collas P. Chrom3D: three-dimensional genome modeling from Hi-C and nuclear lamin-genome contacts. *Genome Biol*. 2017;18:21. doi: 10.1186/s13059-016-1146-2.
18. Lund EG, Duband-Goulet I, Oldenburg A, Buendia B, Collas P. Distinct features of lamin A-interacting chromatin domains mapped by ChIP-sequencing from sonicated or micrococcal nuclease-digested chromatin. *Nucleus*. 2015;6:30–39. doi: 10.4161/19491034.2014.990855.
19. Guelen L, Pagie L, Brasset E, Meuleman W, Faza MB, Talhout W, Eussen BH, de Klein A, Wessels L, de Laat W, van Steensel B. Domain organization of human chromosomes revealed by mapping of nuclear lamina interactions. *Nature*. 2008;453:948–951. doi: 10.1038/nature06947.
20. van Steensel B, Belmont AS. Lamina-associated domains: links with chromosome architecture, heterochromatin, and gene repression. *Cell*. 2017;169:780–791. doi: 10.1016/j.cell.2017.04.022.
21. Gesson K, Rescheneder P, Skoruppa MP, von Haeseler A, Dechat T, Foisner R. A-type lamins bind both hetero- and euchromatin, the latter being regulated by lamina-associated polypeptide 2 alpha. *Genome Res*. 2016;26:462–473. doi: 10.1101/gr.196220.115.
22. Perovanovic J, Dell'Orso S, Gnochi VF, Jaiswal JK, Sartorelli V, Vigouroux C, Mamchaoui K, Mouly V, Bonne G, Hoffman EP. Laminopathies disrupt epigenomic developmental programs and cell fate. *Sci Transl Med*. 2016;8:335ra58. doi: 10.1126/scitranslmed.aad4991.
23. Sullivan T, Escalante-Alcalde D, Bhatt H, Anver M, Bhat N, Nagashima K, Stewart CL, Burke B. Loss of A-type lamin expression compromises nuclear envelope integrity leading to muscular dystrophy. *J Cell Biol*. 1999;147:913–920.
24. Nikolova V, Leimena C, McMahon AC, Tan JC, Chandar S, Jogia D, Kesteven SH, Michalicek J, Otway R, Verheyen F, Rainer S, Stewart CL, Martin D, Feneley MP, Fatkin D. Defects in nuclear structure and function promote dilated cardiomyopathy in lamin A/C-deficient mice. *J Clin Invest*. 2004;113:357–369. doi: 10.1172/JCI19448.
25. Gurha P, Chen X, Lombardi R, Willerson JT, Marian AJ. Knockdown of plakophilin 2 downregulates miR-184 through CpG hypermethylation and suppression of the E2F1 pathway and leads to enhanced adipogenesis in vitro. *Circ Res*. 2016;119:731–750. doi: 10.1161/CIRCRESAHA.116.308422.
26. Lombardi R, Chen SN, Ruggiero A, Gurha P, Czernuszewicz GZ, Willerson JT, Marian AJ. Cardiac fibro-adipocyte progenitors express desmosome proteins and preferentially differentiate to adipocytes upon deletion of the desmoplakin gene. *Circ Res*. 2016;119:41–54. doi: 10.1161/CIRCRESAHA.115.308136.
27. Ruggiero A, Chen SN, Lombardi R, Rodriguez G, Marian AJ. Pathogenesis of hypertrophic cardiomyopathy caused by myozenin 2 mutations is independent of calcineurin activity. *Cardiovasc Res*. 2013;97:44–54. doi: 10.1093/cvr/cvs294.
28. Chen SN, Gurha P, Lombardi R, Ruggiero A, Willerson JT, Marian AJ. The hippo pathway is activated and is a causal mechanism for adipogenesis in arrhythmogenic cardiomyopathy. *Circ Res*. 2014;114:454–468. doi: 10.1161/CIRCRESAHA.114.302810.
29. Karmouch J, Zhou QQ, Miyake CY, Lombardi R, Kretzschmar K, Bannier-Hélaouët M, Clevers H, Wehrens XHT, Willerson JT, Marian AJ. Distinct cellular basis for early cardiac arrhythmias, the cardinal manifestation of arrhythmogenic cardiomyopathy, and the skin phenotype of cardiocutaneous syndromes. *Circ Res*. 2017;121:1346–1359. doi: 10.1161/CIRCRESAHA.117.311876.
30. Marian AJ, Zhao G, Seta Y, Roberts R, Yu QT. Expression of a mutant (Arg92Gln) human cardiac troponin T, known to cause hypertrophic cardiomyopathy, impairs adult cardiac myocyte contractility. *Circ Res*. 1997;81:76–85.
31. Marian AJ, Yu QT, Mann DL, Graham FL, Roberts R. Expression of a mutation causing hypertrophic cardiomyopathy disrupts sarcomere assembly in adult feline cardiac myocytes. *Circ Res*. 1995;77:98–106.
32. Tsybouleva N, Zhang L, Chen S, Patel R, Lutucuta S, Nemoto S, DeFreitas G, Entman M, Carabello BA, Roberts R, Marian AJ. Aldosterone, through novel signaling proteins, is a fundamental molecular bridge between the genetic defect and the cardiac phenotype of hypertrophic cardiomyopathy. *Circulation*. 2004;109:1284–1291. doi: 10.1161/01.CIR.0000121426.43044.2B.
33. Garcia-Gras E, Lombardi R, Giocondo MJ, Willerson JT, Schneider MD, Khoury DS, Marian AJ. Suppression of canonical Wnt/beta-catenin signaling by nuclear plakoglobin recapitulates phenotype of arrhythmogenic right ventricular cardiomyopathy. *J Clin Invest*. 2006;116:2012–2021. doi: 10.1172/JCI27751.
34. Lombardi R, Bell A, Senthil V, Sidhu J, Noseda M, Roberts R, Marian AJ. Differential interactions of thin filament proteins in two cardiac troponin T mouse models of hypertrophic and dilated cardiomyopathies. *Cardiovasc Res*. 2008;79:109–117. doi: 10.1093/cvr/cvn078.
35. Kim D, Pertea G, Trapnell C, Pimentel H, Kelley R, Salzberg SL. TopHat2: accurate alignment of transcriptomes in the presence of insertions, deletions and gene fusions. *Genome Biol*. 2013;14:R36. doi: 10.1186/gb-2013-14-4-r36.
36. Trapnell C, Williams BA, Pertea G, Mortazavi A, Kwan G, van Baren MJ, Salzberg SL, Wold BJ, Pachter L. Transcript assembly and quantification by RNA-Seq reveals unannotated transcripts and isoform switching during cell differentiation. *Nat Biotechnol*. 2010;28:511–515. doi: 10.1038/nbt.1621.
37. Xie X, Lu J, Kulbokas EJ, Golub TR, Mootha V, Lindblad-Toh K, Lander ES, Kellis M. Systematic discovery of regulatory motifs in human promoters and 3' UTRs by comparison of several mammals. *Nature*. 2005;434:338–345. doi: 10.1038/nature03441.
38. Subramanian A, Tamayo P, Mootha VK, Mukherjee S, Ebert BL, Gillette MA, Paulovich A, Pomeroy SL, Golub TR, Lander ES, Mesirov JP. Gene set enrichment analysis: a knowledge-based approach for interpreting genome-wide expression profiles. *Proc Natl Acad Sci USA*. 2005;102:15545–15550.
39. Liberzon A, Subramanian A, Pinchback R, Thorvaldsdóttir H, Tamayo P, Mesirov JP. Molecular signatures database (MSigDB) 3.0. *Bioinformatics*. 2011;27:1739–1740. doi: 10.1093/bioinformatics/btr260.
40. Liberzon A, Birger C, Thorvaldsdóttir H, Ghandi M, Mesirov JP, Tamayo P. The Molecular Signatures Database (MSigDB) hallmark gene set collection. *Cell Syst*. 2015;1:417–425. doi: 10.1016/j.cels.2015.12.004.
41. Kamburov A, Pentchev K, Galicka H, Wierling C, Lehrach H, Herwig R. ConsensusPathDB: toward a more complete picture of cell biology. *Nucleic Acids Res*. 2011;39:D712–D717. doi: 10.1093/nar/gkq1156.
42. Kamburov A, Stelzl U, Lehrach H, Herwig R. The ConsensusPathDB interaction database: 2013 update. *Nucleic Acids Res*. 2013;41:D793–D800. doi: 10.1093/nar/gks1055.
43. Herwig R, Hardt C, Lienhard M, Kamburov A. Analyzing and interpreting genome data at the network level with ConsensusPathDB. *Nat Protoc*. 2016;11:1889–1907. doi: 10.1038/nprot.2016.117.
44. Supek F, Bošnjak M, Škunca N, Šmuc T. REVIGO summarizes and visualizes long lists of gene ontology terms. *PLoS One*. 2011;6:e21800. doi: 10.1371/journal.pone.0021800.
45. Hribal ML, Nakae J, Kitamura T, Shutter JR, Accili D. Regulation of insulin-like growth factor-dependent myoblast differentiation by Foxo forkhead transcription factors. *J Cell Biol*. 2003;162:535–541. doi: 10.1083/jcb.200212107.
46. Renault VM, Thekkat PU, Hoang KL, White JL, Brady CA, Kenzelmann Broz D, Venturelli OS, Johnson TM, Oskoui PR, Xuan Z, Santo EE, Zhang MQ, Vogel H, Attardi LD, Brunet A. The pro-longevity gene FoxO3 is a direct target of the p53 tumor suppressor. *Oncogene*. 2011;30:3207–3221. doi: 10.1038/onc.2011.35.
47. Alkass K, Panula J, Westman M, Wu TD, Guerquin-Kern JL, Bergmann O. No evidence for cardiomyocyte number expansion in preadolescent mice. *Cell*. 2015;163:1026–1036. doi: 10.1016/j.cell.2015.10.035.
48. Schobesberger S, Wright P, Tokar S, Bhargava A, Mansfield C, Glukhov AV, Poulet C, Buzuk A, Monszpart A, Sikkel M, Harding SE, Nikolaev VO, Lyon AR, Gorelik J. T-tubule remodelling disturbs localized β2-adrenergic signalling in rat ventricular myocytes during the progression of heart failure. *Cardiovasc Res*. 2017;113:770–782. doi: 10.1093/cvr/cvx074.
49. Guo Y, VanDusen NJ, Zhang L, Gu W, Sethi I, Guatimosim S, Ma Q, Jardin BD, Ai Y, Zhang D, Chen B, Guo A, Yuan GC, Song LS, Pu WT. Analysis of cardiac myocyte maturation using CASAAV, a platform for rapid dissection of cardiac myocyte gene function in vivo. *Circ Res*. 2017;120:1874–1888. doi: 10.1161/CIRCRESAHA.116.310283.
50. Reynolds JO, Quick AP, Wang Q, Beavers DL, Philippen LE, Showell J, Barreto-Torres G, Thuerauf DJ, Doroudgar S, Glembotski CC, Wehrens XH. Junctophilin-2 gene therapy rescues heart failure by normalizing RyR2-mediated Ca2+ release. *Int J Cardiol*. 2016;225:371–380. doi: 10.1016/j.ijcard.2016.10.021.
51. Donti TR, Stromberger C, Ge M, Eldin KW, Craigen WJ, Graham BH. Screen for abnormal mitochondrial phenotypes in mouse embryonic stem cells identifies a model for succinyl-CoA ligase deficiency and mtDNA depletion. *Dis Model Mech*. 2014;7:271–280. doi: 10.1242/dmm.013466.
52. Liao CY, Anderson SS, Chicoine NH, Mayfield JR, Academia EC, Wilson JA, Pongkietisak C, Thompson MA, Lagmay EP, Miller DM, Hsu YM, McCormick MA, O'Leary MN, Kennedy BK. Rapamycin reverses

metabolic deficits in lamin A/C-deficient mice. *Cell Rep*. 2016;17:2542–2552. doi: 10.1016/j.celrep.2016.10.040.
53. Calnan DR, Brunet A. The foxO code. *Oncogene*. 2008;27:2276–2288. doi: 10.1038/onc.2008.21.
54. Yang L, Jiang J, Drouin LM, Agbandje-McKenna M, Chen C, Qiao C, Pu D, Hu X, Wang DZ, Li J, Xiao X. A myocardium tropic adeno-associated virus (AAV) evolved by DNA shuffling and in vivo selection. *Proc Natl Acad Sci USA*. 2009;106:3946–3951.
55. Prasad KM, Xu Y, Yang Z, Acton ST, French BA. Robust cardiomyocyte-specific gene expression following systemic injection of AAV: in vivo gene delivery follows a poisson distribution. *Gene Ther*. 2011;18:43–52. doi: 10.1038/gt.2010.105.
56. Reay DP, Niizawa GA, Watchko JF, Daood M, Reay JC, Raggi E, Clemens PR. Effect of nuclear factor κB inhibition on serotype 9 adeno-associated viral (AAV9) minidystrophin gene transfer to the mdx mouse. *Mol Med*. 2012;18:466–476. doi: 10.2119/molmed.2011.00404.
57. Falk DJ, Mah CS, Soustek MS, Lee KZ, Elmallah MK, Cloutier DA, Fuller DD, Byrne BJ. Intrapleural administration of AAV9 improves neural and cardiorespiratory function in Pompe disease. *Mol Ther*. 2013;21:1661–1667. doi: 10.1038/mt.2013.96.
58. Smuder AJ, Sollanek KJ, Min K, Nelson WB, Powers SK. Inhibition of forkhead boxO-specific transcription prevents mechanical ventilation-induced diaphragm dysfunction. *Crit Care Med*. 2015;43:e133–e142. doi: 10.1097/CCM.0000000000000928.
59. Milan G, Romanello V, Pescatore F, Armani A, Paik JH, Frasson L, Seydel A, Zhao J, Abraham R, Goldberg AL, Blaauw B, DePinho RA, Sandri M. Regulation of autophagy and the ubiquitin-proteasome system by the FoxO transcriptional network during muscle atrophy. *Nat Commun*. 2015;6:6670. doi: 10.1038/ncomms7670.
60. Cao DJ, Jiang N, Blagg A, Johnstone JL, Gondalia R, Oh M, Luo X, Yang KC, Shelton JM, Rothermel BA, Gillette TG, Dorn GW, Hill JA. Mechanical unloading activates FoxO3 to trigger Bnip3-dependent cardiomyocyte atrophy. *J Am Heart Assoc*. 2013;2:e000016. doi: 10.1161/JAHA.113.000016.
61. Sengupta A, Molkentin JD, Paik JH, DePinho RA, Yutzey KE. FoxO transcription factors promote cardiomyocyte survival upon induction of oxidative stress. *J Biol Chem*. 2011;286:7468–7478.
62. Blice-Baum AC, Zambon AC, Kaushik G, Viswanathan MC, Engler AJ, Bodmer R, Cammarato A. Modest overexpression of FOXO maintains cardiac proteostasis and ameliorates age-associated functional decline. *Aging Cell*. 2017;16:93–103. doi: 10.1111/acel.12543.

Circulation Research
JOURNAL OF THE AMERICAN HEART ASSOCIATION

Suppression of Activated FOXO Transcription Factors in the Heart Prolongs Survival in a Mouse Model of Laminopathies

Gaelle Auguste, Priyatansh Gurha, Raffaella Lombardi, Cristian Coarfa, James T. Willerson and Ali J. Marian

Circ Res. 2018;122:678-692; originally published online January 9, 2018;
doi: 10.1161/CIRCRESAHA.117.312052
Circulation Research is published by the American Heart Association, 7272 Greenville Avenue, Dallas, TX 75231

Print ISSN: 0009-7330. Online ISSN: 1524-4571

Online Supplementary Material

Suppression of Activated FOXO Transcription Factors in the Heart Prolongs Survival in a Mouse Model of Laminopathies

Gaelle Auguste, Ph.D., Priyatansh Gurha, Ph.D., Raffaella Lombardi, M.D., Ph.D., Cristian Coarfa, Ph.D.* James T. Willerson, M.D., Ali J. Marian, M.D.

Center for Cardiovascular Genetics, Institute of Molecular Medicine and Department of Medicine, University of Texas Health Sciences Center at Houston, Texas Heart Institute, and

* Baylor College of Medicine, Houston, TX 77030

Running title: Improved survival upon suppression of FOXO TFs in laminopathies

Address for Correspondence:

AJ Marian, M.D.
Center for Cardiovascular Genetics
6770 Bertner Street
Suite C900A
Houston, TX 77030
713 500 2350
Ali.J.Marian@uth.tmc.edu

METHODS

The studies conformed to the Guide for the Care and Use of Laboratory Animals published by the US National Institutes of Health and were approved by the Animal Care and Use Committee and the Biological Safety Committee of the University of Texas Health Science Center-Houston.

The data, methods used in the analysis, and materials used to conduct the research will be made available to any researcher for purposes of reproducing the results or replicating the procedure. The transcriptomic data will be deposited in NCBI GEO Profile and maintained indefinitely.

***Lmna*$^{-/-}$ and wild type (WT) littermates:** The phenotype in the *Lmna*$^{-/-}$ mice has been published. [1, 2] *Lmna*$^{-/-}$ and age- and sex-matched WT littermate mice were used as controls in these experiments, the latter as controls. Mice were maintained in the C57BL/6 background and housed in a 12-hour light/night cycle facility with *ad libidum* food and water. Genotyping was performed by polymerase chain reaction (PCR) of DNA extracted from tail-clip. Oligonucleotide primers used in PCR reactions are listed in Online Table I.

Mice were euthanized by carbon dioxide inhalation followed by cervical dislocation. Hearts were rapidly excised, rinsed twice with ice-cold Phosphate Buffered Saline (PBS), and dry-blotted before use or storage at -80 °C.

Survival: Survival was analyzed by constructing Kaplan-Meier survival plots.

Gross morphology: Mice were weighted weekly to record body weight (BW). Heart was excised from the chest, after euthanasia, and heart weight/body weight (HW/BW) ratio was calculated in age- and sex-matched littermate mice.

Echocardiography: Cardiac size and function were assessed in age- and sex-matched littermate mice by 2D, M mode, and Doppler echocardiography, as published using a Vevo 1100 ultrasound imaging system equipped with a 22-55 MHz MicroScan transducer (MS550D) (FUJIFILM VisualSonics Inc., Toronto, ON, Canada). [3-6] Echocardiography was performed in 2- and 4-week old WT and *Lmna*$^{-/-}$ littermate mice. In brief, mice were lightly anesthetized by intraperitoneal injection of sodium pentobarbital (60 mg/Kg body weight). After removing the chest fur with a hair removal cream (Nair), mice were positioned

supine on a heating pad with embedded ECG leads. ECG and respiratory rate were recorded during the study**.** Wall thicknesses and left ventricular dimensions were measured from M-mode images from the parasternal two-dimensional short-axis view at the tip of the mitral leaflet, using the leading-edge method. Left ventricular fractional shortening and mass were calculated from the measured indices. Echocardiographic data were measured in 3 cardiac cycles and mean values were used.

Isolation of adult cardiac myocytes: Mice were anesthetized by intra-peritoneal (I.P.) injection of pentobarbital (62 mg/Kg) followed by I.P. injection of heparin (200U) to prevent clot formation.[4] The heart was excised and placed in a Ca^{2+} free perfusion buffer [120 mM NaCl, 15 mM KCl, 0.6 mM KH_2PO_4, 0.6 mM Na_2HPO_4, 1.2 mM $MgSO_47H_2O$, 30 mM Taurine, 4.6 mM $NaHCO_3$, 10 mM HEPES, 10 mM 2,3-Butanedione monoxime (BDM), and 5.5 mM Glucose; pH 7.0]. The heart was cannulated through ascending aorta, the cannula was positioned above the aortic valves, and the heart was connected to a retrograde perfusion system. The heart was perfused with the perfusion buffer at a constant rate of 4 mL/min for 2 minutes, then 250 units/mL of Collagenase II (Worthington, Lakewood, NJ) was added to the buffer, and the perfusion was continued for another 2 minutes. The digestion buffer was then supplemented with 12.5 μM $CaCl_2$; the perfusion was continued until complete softening of the myocardium. The heart was then cut into small pieces in the digestion buffer, and cells were dissociated by gentle pipetting. Upon complete dissociation of the cells, calf serum (10% in final volume) was added to stop the enzymatic digestion, and cells were passed through a 100 μm nylon mesh. Myocytes were left to sediment by gravity in the presence of 2 mM ATP and pelleted by centrifugation at 20 g for 3 min. Sequential concentrations of calcium (100 μM, 400 μM, and 900 μM), were re-introduced to the cells in presence of 2 mM ATP . The final isolate was resuspended in a plating media (MEM media, 1% penicillin-streptomyocin, 10% Calf serum, 10 mM BDM, and 2 mM ATP) and placed on laminin-coated cover glasses in a 2% $_2$ incubator at 37 °C or were immediately frozen.

Isolation of neonatal mouse ventricular myocytes: Hearts from 1- to 2-day old wild-type pups were rapidly excised from the chest. Atria were cut out and pooled ventricules were minsed in ice cold ADS buffer (120 mM NaCl, 5.4 mM KCl, 5.5mM Glucose, 12.5 mM NaH_2PO_4, 0.8 mM $MgSO_4$, and 20mM HEPES, pH = 7.2). Ventricular tissue was digested by successive enzymatic digestions in a buffer containing 70U/mL of Collagenase II (Worthington cat# LS004176) and 0.6mg/mL of pancreatin (Sigma # P3292) at 37 °C. Cell suspension was thereafter purified by pre-plating for 1 hour and half at 37°C, 5% CO_2. Non-adherent cells were then recovered, counted and grown on chamber slides (Corning, 08-774) coated with Poly-D-Lysine (Sigma, # A-003-E) in DMEM supplemented with 10% bovine calf-serum (Gibco, #16170078).

Cells were infected with recombinant adenoviruses expressing a constitutively active FOXO3 or vector adenoviruses (Vector Biolabs, #1025 and #1300) on day 2 at a multiplicity of infection of 20 for 48 hours. In the constitutively active form of FOXO3 ($FOXO3^{AAA}$) three phosphorylation sites (Thr^{32}, Ser^{253} and Ser^{315}) were mutated for alanine. The construct mimicks FOXO3 activation, as observed in the *Lmna*$^{-/-}$ myocytes.

To assess superoxide anion production by the mitochondria, neonatal mouse cardiac myocytes were stained with MitoSOX Red (5 μM; InvitroGen M36008) for 30min according to manufacturer's instructions. Then, cells were fixed and the nuclei were counterstained with DAPI.

Histology: Myocardial histology was examined upon staining of thin (4-5 μm) myocardial sections with Masson trichrome and Sirius Red (SR), as described. [4, 7, 8] Extent of interstitial fibrosis was quantified by determining collagen volume fraction (CVF) in at least 10 high magnification fields (x40) per section and 5 sections per heart. [7] Images were analyzed using the ImageJ software.

Immunofluorescence (IF): IF was performed as previously described. [6, 83] The detailed list of antibodies used is provided in the Supplemental Table I. Briefly, myocardial frozen section were fixed for 15 min at room temperature in 4% formaldehyde. After extensive washes, sections were blocked in 5% donkey serum with PBS-0.3% Triton X-100 for 1 hour at room temperature and then were incubated with the primary antibodies in 1% bovine serum albumin (BSA) in PBS-0.3% Triton-X-100 at 4°C overnight.

Sections were then incubated with appropriate secondary antibodies conjugated with fluorescent dyes. Nuclei were conterstained with 0.1 mg/mL of 4′, 6 Diamidino-2-phenylindole dihydrochloride (DAPI) (Sigma-Aldrich St Louis, MO; cat# D8417). Slides were mounted using fluorescent mounting medium (Dako cat# S3023). Section were then examined with an inverted fluorescent microscope (Zeiss, Axioplan Fluorescence Microscope). Image acquisition was completed with AxioVision software. Nuclear localixation of FOXO3 was determined by counting the number nuclei stained positive for FOXO3 in a minimum of 10 high magnification fields (X40), 2-3 thin sections, per heart, and 3 mice per experimental group (a mimimum of 5,000 nuclei per heart).

Junctophilin (JPH2) and α-actinin (ACTN2) staining were examined on thin frozen section showing myofibrils in the longitudinal axis. Iterative deconvolution was performed on Z-stack acquired images at a very high magnification (X100). A minimum of 5 fields, 2-3 thin sections per heart, and 3 mice per experimental group were examined.

Detection of apoptosis: Apoptosis was detected by nick-end labelling of DNA with the TUNEL assay using In Situ Cell Death Detection Kit (Roche catalogue # 11684795910 and 12156792910), per manufacturer instructions. [4, 9] In brief, formalin fixed-paraffin embedded thin myocardial sections were dewaxed before processing. Simiarly, neonatal mouse cardiac myocytes were fixed for 15 min in 4% paraformaldehyde and processed similarly. Samples were treated with Proteinase K (10 mg/ml in 10 mM Tris/HCl, pH 7.5) for 20 min at 37°C and subsequently incubated with the TUNEL reaction mixture for 1 hour at 37°C. Nuclei were counterstained with DAPI and after extensive washing, coverslips were mounted with anti-fading mounting media (DAKO). Visualization and quantification of apoptotic-positive cells was done under fluorescence microscopy using Axioplan fluorescence microscope (Zeiss). A minimum of 10 high magnification fields (x40) per section, 3-4 thin sections per each heart, and four to five mice per experimental group were examined to determine the percentage of TUNEL-positive nuclei.

Quantitative real-time PCR (qPCR): Total RNA was extracted from myocardial tissue or from isolated cardiac myocytes using the Qiagen miRNeasy Mini Kit (catalogue # 217006). [3, 6] RNA was treated on column containing DNase to eliminate contaminating genomic DNA. The cDNA was synthesized using

High Capacity cDNA Reverse Transcription Kit (Life tech, catalogue # 4368814). Transcript levels were determined by qPCR using specific TaqMan gene expression assays or SYBR Green specific primers, and normalized to glyceraldehyde-3-phosphate dehydrogenase (*Gapdh*) mRNA levels. All reactions were performed in triplicates and in four to six mice per group. The ΔCT method was used to calculate the normalized gene expression value (normalized to *Gapdh*). Data in the experimental groups were presented as fold change relative to the control samples. Taqman probes and SYBR Green primers are detailed in Online Table I.

Immunoblotting: Expression levels of the proteins of interest in mouse heart samples and isolated cardiac myocytes were detected and quantified by immunoblotting, as described. [3, 4, 6] Briefly, tissues were lysed in a RIPA buffer (PIERCE, Rockford, IL, catalogue #89900) containing protease and phosphatase inhibitors (cØmplete and phosSTOP; Roche Molecular Biochemicals, catalogue # 11-873-580-001 and # 04-906-837-001, respectively). The samples were homogenized using a hand-held homogenizer and lysed on a rotator at 4 °C for 20 minutes. The cell debris were pelleted by centrifugation at 12,000 rpm for 15 min at 4 °C. Protein concentration was measured by Bio-Rad DC Protein Assay Kit (Bio-Rad Laboratories, catalogue # 5000111). Protein extracts were heated in a Laemmli buffer at 95 °C for 5 min. Aliquots of 30-50 μg of each protein extract were loaded onto SDS/PAGE gels, separated by electrophoresis, and transferred to nitrocellulose membranes. The membranes were probed with primary antibodies against the proteins of interest and the corresponding HRP conjugated secondary antibodies (the list of the antibodies is provided in Online Table I). Signals were detected by chemiluminescence using the LI-COR Odyssey Fc imaging system (LI-COR Biotechnology). Probes were stripped off the membranes upon incubation in Restore PLUS Western Blot Stripping Buffer (Thermo Scientific, Hudson, New Hampshire, catalogue #46430) at room temperature, and the membranes were reprobed with antibodies against the loading control protein GAPDH or tubulin α1a (TUB1A1). Intensity of the specific bands was quantified using the Image J Studio™ software. Each lane read out was normalized to its corresponding band of the loading control. Data in the experimental groups were presented as the fold change relative to the control samples.

Cell protein sub-fractionation and immunoblotting: Nuclear and cytosolic proteins were extracted using a commercial kit (ProteoExtract®, Calbiochem, catalogue # 539790). [10] All steps were conducted at 4 °C. The hearts were minced and homogenized in a dounce glass homogenizer in 1 mL of a cold Extraction Buffer complemented with protease inhibitors cocktail provided in the kit and with phosphatase inhibitors cocktail, as described above. After incubation and gentle rocking for 20 min, the homogenates were centrifuged at 18,000g for 20 min to pellet the membrane and nuclear fractions and to collect the supernatant containing the cytosolic proteins. After two washes, the pellets were resuspended in 100 µL of an ice-cold buffer containing HEPES (pH7.9), $MgCl_2$, NaCl, EDTA, Glycerol, Sodium OrthoVanadate, plus proteinase inhibitors cocktail. After gentle mixing for 20 min and centrifugation at 18,000g for 20 min, the supernatant containing nuclear proteins was collected.

RNA-Sequencing (RNA-Seq): RNA-sequencing was performed in the whole heart ribosome-depleted RNA extracts from the 2-week old WT and *Lmna*$^{-/-}$ mice on an Illumina platform, as published with minor modifications. [3, 6] In brief, ribosome-depleted RNA was extracted from the whole heart and analyzed for integrity on an Agilent Bioanalyser RNA chip. Samples with a RNA Integrity Number (RIN) read out of more than 8 were used to prepare sequencing library using the Illumina TruSeq stranded total RNA library preparation kit. The samples were sequenced on the Illumina HiSeq 4000 instrument using the paired-end sequencing reagents to generate 100 base pair runs.

Raw RNA sequencing reads were mapped to the Mouse reference genome build 10 (UCSC mm10/GRCm38) by Tophat2. [11] Gene expression was assessed using Cufflinks2 and the GENCODE gene model. [11, 12] Counts were presented as fragments per kilobase of transcript per million mapped fragments (FPKM). Gene expression profiles were normalized using the quantile normalization method as implemented in the R statistical system. Only transcripts that exceeded 1 FPKM in at least one sample were included in the subsequent analyses. Differentially expressed transcripts (DETs) were identified using the edgeR analysis package in R statistical program with the significance level set at $q<0.05$ and the fold change at > 1.25, using the R statistical system. Quality control and data visualization were assessed by principal components analysis (PCA) and hierarchical clustering in R. GENE-E software

(http://www.broadinstitute.org/cancer/software/GENE-E) was used to generate the heatmaps from the raw FPKM values and the Graph Pad Prism was used to generate the volcano plots. Enriched upstream regulators and transcription factor binding sequence motifs were inferred using the following programs: Gene Set Enrichment (GSEA, version 2.2.3, http://software.broadinstitute.org/gsea/); Transcription factor binding motifs TRANSFAC, [13] Molecular Signature Database (MSigDB) using the compute overlap function for transcription factor targets [14-16] and the Ingenuity Pathway Analysis® (IPA, Qiagen). The list of TF target genes dysregulated in the *Lmna*$^{-/-}$ mouse hearts was generated by combining targets identified by GSEA and IPA. Gene Ontology (GO) analyses of FOXO TFs targets genes were conducted using ConsensusPathDB (release MM9-http://cpdb.molgen.mpg.de/MCPDB), [17, 18 19] and GO terms were gathered according to their similarities using REVIGO (http://revigo.irb.hr/). [20] Circos plot was generated in R using the GO-Chord option.

***AAV9-mediated In vivo* suppression of FOXO TFs in the heart:** A short hairpin RNA (shRNA) that has been shown to targets FOXO1 and FOXO3 in independent studies [21, 22] was cloned into AAV9 vectors downstream to a U6 promoter (VectoBiolab). The construct also contained a green fluorescence protein (GFP) expression cassette regulated by a CMV promoter. Control AAV9 vectors contained either a GFP or a scrambled shRNA expression cassette. Sequence of the shRNA against FOXO1 and 3 and scrambled shRNA are presented in Online Table I.

To knock down expression of FOXO1 and FOXO3 in the heart, recombinant AAV9 constructs at a titer of $0.5x10^{11}$ vector genomes per gram of body weight (vg/g) were injected subcutaneously at the nape of the neck into neonatal mice. Three sequential injections at P2, P4, and P6 postnatal days were made, delivering a total of 1.5×10^{11} vg/g to each mouse. Control AAV9 vectors where inject at the same dosage and time points. The early time point was chosen as the *Lmna*$^{-/-}$ have a poor survival rate beyond 4 weeks and almost all die within 8 weeks. [1, 2] Thus, the early injections enabled sufficient time for gene expression through the recombinant AAV9 vectors, prior to the onset of the cardiac phenotype. Serial injections, performed prior to complete immune competency, are expected to enhance transduction efficiency by targeting the newly formed cardiac myocytes in the early neonatal period. [23] The viral titer was chosen

based on the established dose for an efficient transduction of cardiac myocytes while avoiding toxicity. [24-26]

Cytokines measurement: Cytokine and chemokine levels in the heart of 2 weeks old WT and *Lmna*$^{-/-}$ mice were measured using the Milliplex MAP Mouse Cytokine/Chemokine 32-plex assay (Millipore) according to manufacturer's protocol (MCYTMAG-70K-PX32) (Antibody Based Proteomics Core at Baylor College of Medicine, www.bcm.edu/centers/cancer-center/research/shared-resources/antibody-based-proteomics).

Mitochondrial Electron Chain Transport (ETC) Activity: Enzymatic activity of the mitochondrial ETC was assessed in the heart of 2-week old WT and *Lmna*$^{-/-}$ mice, as published. [27] In brief, hearts were homogenized on ice by gentle douncing in a homogenization buffer (120mM KCl, 20mM HEPES, 1mM EGTA, pH7.4), centrifuged at 600g and 4°C for 10 minutes, and the supernatants were used to perform the enzymatic measurements. The specific substrate of each ETC complex was added to the supernatant and the activity was measured by colorimetric assays using a monochromator microplate reader (Tecan M200) at 30 °C in a volume of 175 µL. Complex I activity was determined upon measuring oxidation of NADH at 340 nm using ferricyanide as the electron acceptor in a mixture of 25 mM potassium phosphate (pH 7.5), 0.2 mM NADH, and 1.7 mM potassium ferricyanide (NADH:ubiquinone oxidoreductase). Complex II activity (succinate dehydrogenase) was assessed by determining by the rate of reduction of the artificial electron acceptor 2,6-dichlorophenol-indophenol (DCIP) at 600 nm in a mixture of 25 mM potassium phosphate (pH 7.5), 20 mM succinate, 0.5 mM DCIP, 10 µM rotenone, 2 µg/mL antimycin A, and 2 mM potassium cyanide. Complex III activity (Ubiquinol/cytochrome *C* oxidoreductase) was determined by assessing reduction of cytochrome *C* (C*C*) at 550 nm in a mixture of 25 mM potassium phosphate (pH 7.5), 35 µM reduced decylubiquinone, 15 µM C*C*, 10 µM rotenone, and 2 mM potassium cyanide. Cytochrome C oxidase activity at 550 nm was measured in a mixture of 10 mM potassium phosphate (pH 7.5) and 0.1 mM reduced C*C* to determine Complex IV activity. Finally, reduction of 5,5'-dithiobis (2-nitrobenzoic acid) (DTNB) at 412 nm, which is coupled to the reduction of acetyl-CoA by citrate synthase in the presence of oxaloacetate in a mixture of 10 mM potassium phosphate (pH 7.5), 100

mM DTNB, 50 mM acetyl-CoA, and 250 mM oxaloacetate, was used to determine the Citrate Synthase activity. All activities were calculated as nmoles/min/mg protein, normalized to citrate synthase activity, and expressed as a percentage of WT activity. Experiments were performed on four independent samples for each genotype.

ETC complexes assembly immunoblotting: ETC complexes assembly was assessed by immunoblotting of specific subunit of each of the five ETC complexes using the Total OXPHOS Rodent WB Antibody Cocktail (Abcam, #ab110413). These specific subunits are labil, and therefore, are decreased or not detected when complexes are not assembled. Frozen heart tissue were solubilized in SDS buffer (2% SDS, 10% glycerol, 50 mM Tris pH 6.8, protease inhibitor cØmplete) and centrifuged at 4°C and 13,000 rpm for 5 minutes. Supernatant were collected and protein present were quantified. Aliquotes of 50 mM dithiothreitol were added to 20 µg of proteins before loading onto a 4-15% acrylamide gel for SDS-page electrophoresis. Proteins were then transferred on PVDF membrane by CAPS electroblotting in a buffer containing 10 mM 3-[cyclohexylamino]-1-propane sulfonic acid (Sigma C2632) pH 11 and 10 % Methanol. The membrane was then blocked overnight with PBS-5% milk, probed with 6.0 µg/mL of antibodies cocktail for 24 hours at 4°C before incubation with secondary antibody anti-mouse HRP-conjugated. Chemiluminescence signal was acquired using the LI-COR Odyssey Fc imaging system. Analysis was performed using Image Studio software. Loading control was assessed by staining the membrane with Red Ponceau. Proteins were extracted from 2 animal hearts per experimental group and Rat mitochondrial extract was used as positive control.

ATP measurement: To assess if ATP production was impaired in the *Lmna*$^{-/-}$ mouse heart, ATP was measured using the ATP Assay Kit (Abcam, #ab83355) according to manufacturer's instruction. Briefly, 20mg of frozen heart tissue were homogenized on ice using a hand-held homogeneizer in ice-cold 2M Perchloric acid (PCA). Homogenate were then incubated on ice for 45 min before centrifugation at 13,000 g for 2 min at 4°C. Supernatant were collected and PCA neutralized with of ice-cold 2M KOH. pH of the samples was measured and adjusted as necessary to range between 6.5 and 8. Samples were then

centrifugated again at 13,000 g for 2 min at 4°C and used for the colorimetric assay. 5 samples of heart tissue were used per experimental group.

Statistical analyses: Data that followed a Gaussian distribution pattern were presented as mean ± SEM and were compared by t-test and one-way ANOVA. Otherwise, data were presented as the median values and compared by Kruskall-Wallis test, as were the categorical data. Survival rates were analyzed by constructing Kaplan-Meier survival plots and comparing the survival rate by Log-rank (Mantel-Cox) test.

REFERENCES

1. Sullivan T, Escalante-Alcalde D, Bhatt H, Anver M, Bhat N, Nagashima K, Stewart CL, Burke B. Loss of a-type lamin expression compromises nuclear envelope integrity leading to muscular dystrophy. *The Journal of cell biology*. 1999;147:913-920
2. Nikolova V, Leimena C, McMahon AC, Tan JC, Chandar S, Jogia D, Kesteven SH, Michalicek J, Otway R, Verheyen F, Rainer S, Stewart CL, Martin D, Feneley MP, Fatkin D. Defects in nuclear structure and function promote dilated cardiomyopathy in lamin a/c-deficient mice. *The Journal of clinical investigation*. 2004;113:357-369
3. Gurha P, Chen X, Lombardi R, Willerson JT, Marian AJ. Knockdown of plakophilin 2 downregulates mir-184 through cpg hypermethylation and suppression of the e2f1 pathway and leads to enhanced adipogenesis in vitro. *Circulation research*. 2016;119:731-750
4. Lombardi R, Chen SN, Ruggiero A, Gurha P, Czernuszewicz GZ, Willerson JT, Marian AJ. Cardiac fibro-adipocyte progenitors express desmosome proteins and preferentially differentiate to adipocytes upon deletion of the desmoplakin gene. *Circulation research*. 2016;119:41-54
5. Ruggiero A, Chen SN, Lombardi R, Rodriguez G, Marian AJ. Pathogenesis of hypertrophic cardiomyopathy caused by myozenin 2 mutations is independent of calcineurin activity. *Cardiovascular research*. 2013;97:44-54
6. Chen SN, Gurha P, Lombardi R, Ruggiero A, Willerson JT, Marian AJ. The hippo pathway is activated and is a causal mechanism for adipogenesis in arrhythmogenic cardiomyopathy. *Circulation research*. 2014;114:454-468
7. Tsybouleva N, Zhang L, Chen S, Patel R, Lutucuta S, Nemoto S, DeFreitas G, Entman M, Carabello BA, Roberts R, Marian AJ. Aldosterone, through novel signaling proteins, is a fundamental molecular bridge between the genetic defect and the cardiac phenotype of hypertrophic cardiomyopathy. *Circulation*. 2004;109:1284-1291
8. Karmouch J, Zhou QQ, Miyake CY, Lombardi R, Kretzschmar K, Bannier-Helaouet M, Clevers H, Wehrens XHT, Willerson JT, Marian AJ. Distinct cellular basis for early cardiac arrhythmias, the cardinal manifestation of arrhythmogenic cardiomyopathy, and the skin phenotype of cardiocutaneous syndromes. *Circulation research*. 2017;121:1346-1359
9. Garcia-Gras E, Lombardi R, Giocondo MJ, Willerson JT, Schneider MD, Khoury DS, Marian AJ. Suppression of canonical wnt/beta-catenin signaling by nuclear plakoglobin recapitulates phenotype of arrhythmogenic right ventricular cardiomyopathy. *The Journal of clinical investigation*. 2006;116:2012-2021
10. Lombardi R, Bell A, Senthil V, Sidhu J, Noseda M, Roberts R, Marian AJ. Differential interactions of thin filament proteins in two cardiac troponin t mouse models of hypertrophic and dilated cardiomyopathies. *Cardiovascular research*. 2008;79:109-117

11. Kim D, Pertea G, Trapnell C, Pimentel H, Kelley R, Salzberg SL. Tophat2: Accurate alignment of transcriptomes in the presence of insertions, deletions and gene fusions. *Genome Biol*. 2013;14:R36
12. Trapnell C, Williams BA, Pertea G, Mortazavi A, Kwan G, van Baren MJ, Salzberg SL, Wold BJ, Pachter L. Transcript assembly and quantification by rna-seq reveals unannotated transcripts and isoform switching during cell differentiation. *Nat Biotechnol*. 2010;28:511-515
13. Xie X, Lu J, Kulbokas EJ, Golub TR, Mootha V, Lindblad-Toh K, Lander ES, Kellis M. Systematic discovery of regulatory motifs in human promoters and 3' utrs by comparison of several mammals. *Nature*. 2005;434:338-345
14. Subramanian A, Tamayo P, Mootha VK, Mukherjee S, Ebert BL, Gillette MA, Paulovich A, Pomeroy SL, Golub TR, Lander ES, Mesirov JP. Gene set enrichment analysis: A knowledge-based approach for interpreting genome-wide expression profiles. *Proceedings of the National Academy of Sciences of the United States of America*. 2005;102:15545-15550
15. Liberzon A, Subramanian A, Pinchback R, Thorvaldsdottir H, Tamayo P, Mesirov JP. Molecular signatures database (msigdb) 3.0. *Bioinformatics*. 2011;27:1739-1740
16. Liberzon A, Birger C, Thorvaldsdottir H, Ghandi M, Mesirov JP, Tamayo P. The molecular signatures database (msigdb) hallmark gene set collection. *Cell Syst*. 2015;1:417-425
17. Kamburov A, Pentchev K, Galicka H, Wierling C, Lehrach H, Herwig R. Consensuspathdb: Toward a more complete picture of cell biology. *Nucleic Acids Res*. 2011;39:D712-717
18. Kamburov A, Stelzl U, Lehrach H, Herwig R. The consensuspathdb interaction database: 2013 update. *Nucleic Acids Res*. 2013;41:D793-800
19. Herwig R, Hardt C, Lienhard M, Kamburov A. Analyzing and interpreting genome data at the network level with consensuspathdb. *Nat Protoc*. 2016;11:1889-1907
20. Supek F, Bosnjak M, Skunca N, Smuc T. Revigo summarizes and visualizes long lists of gene ontology terms. *PloS one*. 2011;6:e21800
21. Hribal ML, Nakae J, Kitamura T, Shutter JR, Accili D. Regulation of insulin-like growth factor-dependent myoblast differentiation by foxo forkhead transcription factors. *The Journal of cell biology*. 2003;162:535-541
22. Renault VM, Thekkat PU, Hoang KL, White JL, Brady CA, Kenzelmann Broz D, Venturelli OS, Johnson TM, Oskoui PR, Xuan Z, Santo EE, Zhang MQ, Vogel H, Attardi LD, Brunet A. The pro-longevity gene foxo3 is a direct target of the p53 tumor suppressor. *Oncogene*. 2011;30:3207-3221
23. Alkass K, Panula J, Westman M, Wu TD, Guerquin-Kern JL, Bergmann O. No evidence for cardiomyocyte number expansion in preadolescent mice. *Cell*. 2015;163:1026-1036
24. Schobesberger S, Wright P, Tokar S, Bhargava A, Mansfield C, Glukhov AV, Poulet C, Buzuk A, Monszpart A, Sikkel M, Harding SE, Nikolaev VO, Lyon AR, Gorelik J. T-tubule remodelling disturbs localized beta2-adrenergic signalling in rat ventricular myocytes during the progression of heart failure. *Cardiovascular research*. 2017;113:770-782
25. Guo Y, VanDusen NJ, Zhang L, Gu W, Sethi I, Guatimosim S, Ma Q, Jardin BD, Ai Y, Zhang D, Chen B, Guo A, Yuan GC, Song LS, Pu WT. Analysis of cardiac myocyte maturation using casaav, a platform for rapid dissection of cardiac myocyte gene function in vivo. *Circulation research*. 2017
26. Reynolds JO, Quick AP, Wang Q, Beavers DL, Philippen LE, Showell J, Barreto-Torres G, Thuerauf DJ, Doroudgar S, Glembotski CC, Wehrens XH. Junctophilin-2 gene therapy rescues heart failure by normalizing ryr2-mediated ca2+ release. *International journal of cardiology*. 2016;225:371-380
27. Donti TR, Stromberger C, Ge M, Eldin KW, Craigen WJ, Graham BH. Screen for abnormal mitochondrial phenotypes in mouse embryonic stem cells identifies a model for succinyl-coa ligase deficiency and mtdna depletion. *Disease models & mechanisms*. 2014;7:271-280

Online Table I

A. List of primers

Gene Identity	Ref/Oligonucleotidic Sequence
Taqman probes:	
Gapdh	Mm99999915-g1
Tgfb1	Mm01178820-m1
Ctgf	Mm01192932-g1
Col3a1	Mm01254476-m1
Col1a1	Mm00801666-g1
SYBR Green primers:	
***Lmna*-WT**	fwd: 5'- TGGCGGTAGAGGAAGTCGATGAAG-3' rev 5'AGGAAGGAGGACAGGGAGTTCAAC-3'
***Lmna*-KO**	fwd 5'-GGCGGTAGAGGAAGTCGATGAAG-3' rev 5'-TGACCCATGGCGATGCCTGCTTG-3'
Fkbp5	fwd 5'- TCCACTACAAAGGGATGTTGTCA-3' rev 5'-CGAGCCATAAGCATATTCTGGTT-3'
Myl4	fwd 5'-AAGAAACCCGAGCCTAAGAAGG-3' rev 5'-TGGGTCAAAGGCAGAGTCCT-3'
Prg4	fwd 5'- CAGGTTTCATCTCAAGATTT-3' rev 5'- TGTAGTGCAGACTCTCTTGA-3'
Atf3	fwd 5'-CCCCTGGAGATGTCAGTCAC-3' rev 5'- CGGTGCAGGTTGAGCATGT-3'
Hmox1	fwd 5'-CATGAAGAACTTTCAGAAGGG-3' rev 5'-TAGATATCTGACCCAGTTC-3'
Myh7	fwd 5'- ACTGTCAACACTAAGAGGGTCA-3' rev 5'- TTGGATGATTTGATCTTCCAGGG-3'
Psat1	fwd 5'-AAGCCACCAAGCAAGTGGTTA-3' rev 5'-GATGCCGAGTCCTCTGTAGTC-3'
Abi3bp	fwd 5'- TTGAAAGTGCACATCAATAC-3' rev 5'- ACTACAGCCTCTGTGAATTT-3'
Btg2	fwd 5'- ATGAGCCACGGGAAGAGAAC-3' rev 5'- AGCGCCCTACTGAAAACCTTG-3'
Myc	fwd 5'- CTGCTCTCCATCCTATGTT-3' rev 5'- AGTAACTCGGTCATCATCTC-3'
Cryba4	fwd 5'- GGGTGGCAACACAGCCTAC-3' rev 5'- TTGAGTCGCGGTGGTTAGC-3'
Lrtm1	fwd 5'-AAGGACAACCCTTGGATTTGTG-3' rev 5'-ACAGTTCGTGAGGAATGGAGAG-3'
Itgb6	fwd 5'-CAGGTCCGCCAAACTGAAGAT-3' rev 5'-TGTTGAGGTCGTCATCCATAGA-3'

Aurka	fwd 5'-GAGAGTTGAAGATTGCAGAC-3' rev 5'-TAGGAACTCATAGCAGAGAAC-3'
Lmna	fwd 5'- TCCCACCGAAGTTCACCCTA-3' rev 5'- TGGAGTTGATGATGAGAGCGGTG-3'
Cxcl1	fwd 5'- CTGGGATTCACCTCAAGAACATC-3' rev 5'- CAGGGTCAAGGCAAGCCTC-3'
Cxcl2	fwd 5'- ACAGAAGTCATAGCCACTCT-3' rev 5'- ACATCAGGTACGATCCAG-3'
Ccl2	fwd 5'- AAGCTGTAGTTTTTGTCACC-3' rev 5'- TGCATTAGCTTCAGATTTAC-3'
Il6	fwd 5'- GTCTTCTGGAGTACCATAGC-3' rev 5'- GCTTATCTGTTAGGAGAGCA-3'
Lif	fwd 5'- ATTGTGCCCTTACTGCTGCTG-3' rev 5'- GCCAGTTGATTCTTGATCTGGT-3'
Ndufaf1	fwd 5'- TTTGTGGGTAGTCACTGTGTAGA-3' rev 5'- TGTCCTTGTAAGCCCTCTTCAG-3'
Ccnb1	fwd 5'- AAGGTGCCTGTGTGTGAACC-3' rev 5'-GTCAGCCCCATCATCTGCG-3'
Ccnb2	fwd 5'-CCAAGTCCATTCCAAGTTTC-3' rev 5'-CATCTCCTCATATTTGGAAGC-3'
Cdkn1a	fwd 5'- CCTGGTGATGTCCGACCTG-3' rev 5'- CCATGAGCGCATCGCAATC-3'
Foxo1	fwd 5'- CCCAGGCCGGAGTTTAACC-3' rev 5'- GTTGCTCATAAAGTCGGTGCT-3'
Foxo3	fwd 5'- CTGGGGGAACCTGTCCTATG -3' rev 5'-TCATTCTGAACGCGCATGAAG -3'
Foxo4	fwd 5'- CTTCCTCGACCAGACCTCG-3' rev 5'-ACAGGATCGGTTCGGAGTGT-3'
Slc24a2	fwd 5'- GACAAGATTCGAGATTACACCCC-3' rev 5'-TGCAGAATGATGGCACCTTTC-3'
Nr4a2	5'- GTGTTCAGGCGCAGTATGG-3' rev 5'-TGGCAGTAATTTCAGTGTTGGT-3'
Rasgef1b	fwd 5'-TCTGGAAGCCCTTATCCAACA -3' rev 5'-GTGGCAAACCTTAGCCATGAG-3'
Gadd45b	fwd 5'-CAACGCGGTTCAGAAGATGC-3' rev 5'-GGTCCACATTCATCAGTTTGGC-3'
Sqstm1	fwd 5'-ATGTGGAACATGGAGGGAAGA-3' rev 5'-GGAGTTCACCTGTAGATGGGT-3'
Per1	fwd 5'-TGAAGCAAGACCGGGAGAG -3' rev 5'-CACACACGCCGTCACATCA -3'
Etv5	fwd 5'-TCAGTCTGATAACTTGGTGCTTC-3' rev 5'-GGCTTCCTATCGTAGGCACAA-3'
Nfkbia	fwd 5'-TGAAGGACGAGGAGTACGAGC-3' rev 5'-TTCGTGGATGATTGCCAAGTG-3'
Nr4a1	fwd 5'-CTCCCCGAGCCAGACTTATGA-3' rev 5'-TGTCACGGTTCGGAGAGGT-3'
Junb	fwd 5'-CTATCGGGGTCTCAAGGGTC-3' rev 5'-CTGTTGGGGACGATCAAGC-3'
Mt2	fwd 5'-GCCTGCAAATGCAAACAATGC -3' rev 5'-AGCTGCACTTGTCGGAAGC-3'

Maff	fwd 5'-TGGATCCCTTATCTAGCA -3' rev 5'-CTCGGACTTCTGCTTCT-3'
Gabarapl1	fwd 5'-GGACCACCCCTTCGAGTATC-3' rev 5'-CCTCTTATCCAGATCAGGGACC-3'
Cited2	fwd 5'-CGCCAGGTTTAACAACTCCCA-3' rev 5'-TGCTGGTTTGTCCCGTTCAT-3'
Bcl2l11	fwd 5'-CCCGGAGATACGGATTGCAC-3' rev 5'-GCCTCGCGGTAATCATTTGC-3'
Bbc3	fwd 5'-ACGACCTCAACGCGCAGTACG-3' rev 5'-GTAAGGGGAGGAGTCCCATGAAG-3'
Bcl6	fwd 5'-CCGGCACGCTAGTGATGTT-3' rev 5'-TGTCTTATGGGCTCTAAACTGCT-3'
Tnfsf10	fwd 5'- ATGGTGATTTGCATAGTGCTCC-3' rev 5'-GCAAGCAGGGTCTGTTCAAGA-3'
Ndufaf1	fwd 5'- TTTGTGGGTAGTCACTGTGTAGA -3' rev 5'- TGTCCTTGTAAGCCCTCTTCAG -3'
Ndufaf4	fwd 5'- CACCGGAGTCAGTATCCAGAA -3' rev 5'- GGTTCAACTTTTACCGGCAAGG -3'
Ndufs4	fwd 5'- CTGCCGTTTCCGTCTGTAGAG -3' rev 5'- TGTTATTGCGAGCAGGAACAAA -3'
Ndufaf3	fwd 5'- ATGGCTACTGCTCTAGGATTTCG -3' rev 5'- CCGCTGGTATAACTCATCGTC -3'
Ndufs8	fwd 5'- AGTGGCGGCAACGTACAAG -3' rev 5'- TCGAAAGAGGTAACTTAGGGTCA -3'
Ndufb2	fwd 5'- CCCCGGTACAGGGAGTTTC -3' rev 5'- GCCAAAATCGCCAAAGAATCCA -3'
Ndufb10	fwd 5'- GATTCTTGGGACAAGGATGTGT -3' rev 5'- CCTTCGTCAAGTAGGTGATGGG -3'
Ndufs1	fwd 5'- AGGATATGTTCGCACAACTGG -3' rev 5'- TCATGGTAACAGAATCGAGGGA -3'
Ndufa2	fwd 5'- TTGCGTGAGATTCGCGTTCA -3' rev 5'- ATTCGCGGATCAGAATGGGC -3'
Ndufa3	fwd 5'- ATGGCCGGGAGAATCTCTG -3' rev 5'- AGGGGCTAATCATGGGCATAAT -3'
Gapdh	fwd 5'- TGGCAAAGTGGAGATTGTTGC-3' rev 5'-AAGATGGTGATGGGCTTCCCG-3'

B. List of Antibodies

Antibodies	**Supplier**	**Reference**
LMNA	Abcam	# 26300
Emerin (FL-254)	Santa Cruz Biotechnology	# sc-15378
TUB1A1 (11H10)	Cell Signaling Technology	# 21252
GAPDH	Abcam	# 82245
FOXO3 (D19D7)	Cell Signaling Technology	# 12829

FOXO3 (75D8)	Cell Signaling Technology	#2497
FOXO1 (C29H4)	Cell Signaling Technology	# 2880
phosphoFOXO (4G6)	Cell Signaling Technology	# 2599
FOXO4	ProteinTech	21535-1-AP
ACTN2	Sigma	A7811
JPH2	Invitrogen	#40-5300

Anti-Rabbit IgG, Alexa Fluor 594	Life technology	21207
Anti-Mouse IgG, Alexa Fluor 488	Life technology	21202
Anti-rabbit IgG HRP linked antibody	Cell Signaling Technology	# 7074
Anti-mouse IgG HRP linked antibody	Cell Signaling Technology	# 7076

C. ShRNA sequence

FOXO1 and 3 shRNA sequence: 5’- GGATAAGGGCGACAGCAAC-3’

Scrambled-shRNA sequence: 5'-CAACAAGATGAAGAGCACCAA-3'

Online Table II

Echocardiographic variables in 2-week old control wild type and *Lmna*$^{-/-}$ Mice

	WT	*Lmna* $^{-/-}$	*p*
N	15	14	N/A
M/F	9/6	9/5	1.000
Age (days)	13.5 ± 1.3	13.7 ± 1.3	0.708
Body weight (g)	7.08 ± 1.6	5.9 ± 1.3	0.037
HR (bpm)	506 ± 63	512 ± 76	0.839
IVST(mm)	0.55 ± 0.08	0.52 ± 0.08	0.356
PWT (mm)	0.57 ± 0.09	0.53 ± 0.08	0.209
LVEDD (mm)	2.48 ± 0.31	2.37 ± 0.33	0.377
LVEDDi (mm/g)	0.36 ± 0.06	0.41 ± 0.06	0.032
LVESD (mm)	1.22 ± 0.19	1.22 ± 0.26	0.979
LVESDi (mm/g)	0.18 ± 0.03	0.21 ± 0.04	0.059
FS (%)	51.03 ± 2.92	49.17 ± 5.12	0.248
LVM (mg)	32.66 ± 11.95	27.81 ± 9.67	0.248
LVMi (mg/g)	4.71 ± 1.46	4.76 ± 1.52	0.938

Abbreviations: HR: heart rate; bpm: beats per minutes; IVST: interventricular septal thickness; PWT: posterior wall thickness; LVEDD: left ventricular end diastolic diameter; LVEDDi: LVEDD divided by the body weight; LVESD: left ventricular end systolic diameter; LVESDi: LVESD divided for the body weight; FS: fractional shortening; LVM: left ventricular mass; LVMi: LVM divided by the body weight.

Online Table III

Enrichment of conserved cis-regulatory motifs in Differentially Expressed Transcripts

Enrichment of conserved *cis*-regulatory motifs in up-regulated DETs

TFs name	Gene Set Name	Binding motif	Description	# Genes in Overlap (k)	FDR
FOXO4	V$FOXO4_01	TTGTTT	Promoter regions containing the motif TTGTTT which matches annotation for MLLT7: myeloid/lymphoid or mixed-lineage leukemia (trithorax homolog, Drosophila); translocated to, 7	99	1.19E-33
NFAT	V$NFAT_Q4_01	TGGAAA	Promoter regions containing the motif TGGAAA which matches annotation for NFAT:NFATC	80	3.92E-23
AP1	V$AP1_C	TGANTCA	Promoter regions containing the motif TGANTCA which matches annotation for JUN: jun oncogene	60	4.41E-22
E12	V$E12_Q6	CAGGTG	Promoter regions containing the motif CAGGTG which matches annotation for TCF3: transcription factor 3 (E2A immunoglobulin enhancer binding factors E12/E47)	88	8.43E-21
Unknown	UNKNOWN	AACTTT	Promoter regions containing motif AACTTT. Motif does not match any known transcription factor	74	1.03E-19
FREAC2	V$FREAC2_01	RTAAACA	Promoter regions containing the motif RTAAACA which matches annotation for FOXF2: forkhead box F2	51	1.64E-19
AP4	V$AP4_Q5	CAGCTG	Promoter regions containing the motif CAGCTG which matches annotation for REPIN1: replication initiator 1	61	1.45E-16
MAZ	V$MAZ_Q6	GGGAGGRR	Promoter regions containing the motif GGGAGGRR which matches annotation for MAZ: MYC-associated zinc finger protein (purine-binding transcription factor)	74	1.91E-15
PAX4	V$PAX4_03	GGGTGGRR	Promoter regions containing the motif GGGTGGRR which matches annotation for PAX4: paired box gene 4	54	2.01E-15
TATA	V$TATA_01	TATAAA	Promoter regions containing the motif TATAAA which matches annotation for TAF:TATA	54	2.01E-15

Enrichment of conserved *cis*-regulatory motifs indown-regulated DETs

TFs name	Gene Set Name	Binding motif	Description	# Genes in Overlap (k)	FDR
E2F	V$E2F_Q6	TTTSGCGS	Promoter regions containing motif TTTSGCGS. Motif does not match any known transcription factor	9	4.08E-04
E2F	V$E2F_Q4	TTTSGCGS	Promoter regions containing motif TTTSGCGS. Motif does not match any known transcription factor	9	4.08E-04
Unknown	UNKNOWN	TTTNNANAGCYR	Promoter regions containing motif TTTNNANAGCYR. Motif does not match any known transcription factor	7	5.36E-04
NF1	V$NF1_Q6	TGCCAAR	Promoter regions containing the motif TGCCAAR which matches annotation for NF1: neurofibromin 1 (neurofibromatosis, von Recklinghausen disease, Watson	14	7.74E-04
E2F1-DP1-RB	V$E2F1_Q4_01	TTTSGCGSG	Promoter regions containing the motif TTTSGCGSG which matches annotation for E2F;TFDP1: transcription factor Dp-1	8	7.74E-04
E2F1-DP1-RB	V$E2F1DP1RB_01	TTTSGCGC	Promoter regions containing the motif TTTSGCGC which matches annotation for E2F1: E2F transcription factor 1; TFDP1: transcription factor Dp-1;RB1: retinoblastoma 1 (including osteosarcoma)	8	7.74E-04
E2F1-DP1-RB	V$E2F1DP2_01	SGCGSSAAA	Promoter regions containing the motif SGCGSSAAA which matches annotation for E2F1: E2F transcription factor 1;TFDP1: transcription factor Dp-1;RB1: retinoblastoma 1 (including osteosarcoma)	7	7.74E-04
Unknown	UNKNOWN	KRCTCNNNNMANAGC	Promoter regions containing motif KRCTCNNNNMANAGC. Motif does not match any known transcription factor	5	7.74E-04
E2F	V$E2F_Q3_01	TTTSGCGSG	Promoter regions containing the motif TTTSGCGSG which matches annotation for E2F:TFDP1: transcription factor Dp-1	8	7.74E-04
E2F	V$E2F_Q4_01	NCSCGCSAAAN	Promoter regions containing the motif NCSCGCSAAAN which matches annotation for E2F:TFDP1: transcription factor Dp-1	8	7.74E-04

Up and down-regulated DETs were analysed for enrichment of conserved upstream cis-regulatory motifs by using the MSigDB from GSEA. The conserved transcription factor binding sites and conserved motifs analysis was restricted to the promoter region around transcription start site (4kb window, -2 kb; +2kb).

Top ten of the significantly over-represented *cis*-regulatory motifs are presented in the tables. Over-representation is calculated by hypergeometric distribution of overlapping genes (k) over all genes in the gene universe, after correction for multiple hypothesis testing.

Online Table IV

Upstream regulators of DETs in *Lmna*$^{-/-}$ mice predicted by IPA.

Predicted Activation State	IPA ranking	Upstream Regulator	Activation z-score	p-value of overlap	Target molecules in dataset
Activated	1	CTNNB1	4.577	6.48E-12	APOD,BCL2,BCL2L1,C2orf40,CA3,CD44,CDKN1A,CTGF,CYP1B1,CYR61,DPEP1,EYA2,F2R,FAS,FOXC1,FOXC2,FSTL3,FZD7,GADD45B,GDNF,GLUL,ID4,KLF5,LGALS3,MME,MMP3,MYC,MYCN,MYL4,NR4A1,NR5A2,PCCA,PRDM1,PRSS35,SERPINA3,SERPINE1,SGK1,SLC1A5,SMAD6,SOX17,SPP1,SQSTM1,SYNM,TGFA,TIMP3,TNFRSF19,VCAM1,WIF1,WNT11
	2	CREB1	4.03	2.73E-14	ATF3,AURKA,BCL2,BCL2L1,BTG2,CCNB1,CCNB2,CEBPD,CSRNP1,CYR61,EGR1,ENTPD1,ERRFI1,FOS,FOSB,GADD45B,IRS2,JUNB,KLF5,MIDN,MKI67,MYC,NR4A1,NR4A2,NR4A3,PER1,PPP1R15A,Retnla,Sik1
	3	CREM	3.762	1.18E-09	ATF3,BTG2,CSRNP1,EGR1,ERRFI1,FOS,GADD45B,HAND2,IRS2,JUNB,KLF5,MIDN,NR4A1,NR4A2,PER1,PPP1R15A,RYR2,Sik1,STAR,THBS1
	4	FOXO3	3.755	3.26E-07	Acot1,BNIP3,CDKN1A,CTGF,EGR1,FOS,FOSB,GADD45B,GSTM5,JUNB,LCN2,Mt1,Mt2,NFKBIA,SGK1,
	5	TP53	3.507	3.27E-20	ABCG2,ACER2,ADAM8,ATF3,AURKA,BCL2,BCL2L1,BMX,BNIP3,BTG2,CAMK2N1,Ccl2,CCNB1,CDC7,CDKN1A,CEP55,CITED2,CKAP2,CLU,COL2A1,CTGF,DDIT4,DKK3,DPEP1,DUSP5,EGR1,ENPP2,EPHX1,F2R,FAS,FHL1,FKBP4,FKBP5,FOS,FSTL3,GDF15,GLUL,GNA13,GNL3,GPX3,GSTM5,Hist1h1b,HK2,HMOX1,HRASLS,HSPA1A/HSPA1B,HSPB1,HSPD1,IFI16,IGF1R,IGF2,IGFBP3,IL16,JUNB,KDR,KRT18,KRT8,LGALS3,LOC102724788/PRODH,LOX,MCM2,MIR17HG,MKI67,MMP3,MPZL2,Mt2,MYC,MYL4,NFKBIA,PCCA,PEG10,PERP,PFKFB3,PHLDA1,PHLDA3,PIM1,POLD2,PRC1,PRDM1,PTGDS,PTGS1,PTPRU,RAD51,RBM3,SELP,SERPINA3,SERPINE1,SERPINH1,SGK1,SHROOM3,SLC2A12,SLC6A6,SMAD6,SPHK1,SPP1,TGFA,TGFB2,THBS1,TIMP3,TMEM151A,TMEM43,TNFAIP8,TOP2A,TP53INP1,TPX2,TTK,UHRF1,UNG
	6	EGR1	3.373	8.5E-10	ATF3,CACNA1H,Ccl2,CD44,CDKN1A,CHGB,CXCL3,EREG,FAS,FTL,GDF15,HMOX1,HPSE,IGF2,JUNB,JUND,MYC,SERPINE1,THBS1,VCAM1
	7	ATF4	3.215	8.22E-09	ANGPTL3,ANKRD1,ATF3,CDKN1A,CHAC1,DDIT4,EIF4EBP1,GDF15,LGALS3,MGST1,OSMR,PCK1,PSAT1,PTX3,SLC1A5,SLC38A2,SLC38A3,SLC3A2,SLC7A5,WNT11
	8	RELA	3.102	4.29E-08	ABCG2,ANKRD1,BCL2,BCL2L1,BTG2,CBS/CBSL,Ccl2,CD14,CD44,CDKN1A,CITED2,CXCL3,CXCR4,CYP2B6,FAS,FOS,HMOX1,MYC,NFKBIA,NR4A1,PRDM1,PRKCD,PTGDS,PTX3,SDC4,SLC2A5,VCAM1
	9	SMAD3	3.064	0.0000106	ANKRD1,BCL2,Ccl2,CDKN1A,COL2A1,CTGF,CXCL3,EREG,FOS,FSTL3,JUNB,JUND,MYC,SERPINE1,SPHK1,TGFA,TIMP3
	10	ID2	2.813	0.000929	BCL2,BCL2L1,CCNB1,CD19,CD44,CDKN1A,CXCR4,CXCR6,GADD45B,KLF6,MYC,NR4A1,NR4A3,RAP1GAP
	...				
	29	FOXO4	2.215	0.00513	BNIP3,CDKN1A,CTGF,GADD45B,SGK1
	...				
	96	FOXO1	0.616	2.72E-08	ASPM,BCL2,CCNB1,CCNB2,CDKN1A,CTGF,DEPDC1,DLGAP5,EGR1,FOS,FOSB,GADD45B,GCK,IGF1R,IRS2,ITGA3,ITGB6,JUNB,MMP3,MRPL45,MYC,NDUFAF1,PCK1,PRC1,PRDM1,SGK1,THBS1,UCP1,VCAM1
Inhibited	9	MKL2	-2	0.00000312	BCL2L1,CLDN15,CXCR4,DMKN,EYA2,F2R,GSTM5,Ifitm1,LCN2,MAFK,P2RY1,SELP,SERINC3
	8	HLX	-2.121	6.86E-07	ANKRD1,CCNB1,CYP1B1,EGR1,GDF15,MYC,PAPPA,PRDM1
	7	BACH1	-2.15	0.000246	CXCR4,GCLM,HMOX1,SPP1,SQSTM1
	6	HEY2	-2.193	0.000324	ANKRD1,MYL4,MYL7,NPPA,SLN
	5	SNAI2	-2.219	0.0034	ANKRD1,COL2A1,CTGF,CYR61,ITGA3
	4	GMNN	-2.646	0.00524	CDKN1A,CITED1,DUSP5,FOXF1,IRX3,SOX17,TGFB2,TNFRSF19
	3	SOX1	-2.646	0.00947	CITED1,DUSP5,FOXF1,IRX3,SOX17,TGFB2,TNFRSF19
	2	HOXA10	-3	0.00592	ADM,CA3,ENPP2,IGFBP3,INMT,LCN2,MYCN,NR4A1,XDH
	1	SOX2	-3.443	0.00000136	ATF3,CITED1,CITED2,CTGF,CXCR4,DUSP5,ESRRB,ETV5,FOXF1,GADD45B,GATA6,GCK,GRHL3,H19,IRX3,KDR,KLF6,KRT18,MYCN,NR5A2,PRDM1,PRKCD,SOX17,TGFB2,TIMP3,TNFRSF19

Differentially Expressed Transcripts were analysed using Ingenuity Pathway Analysis (IPA) Software to predict upstream transcriptional regulators under the most stringent setting. Significant upstream regulators are identified based on the literature and curated IPA database. A Fisher's Exact Test p-value calculation of the overlap between the DETs and known targets render the significant overrepresented upstream regulator. Prediction of regulators activation state is inferred based on the direction of the change of knowns target, consistent with the literature and is computed by z-score. In the table are displayed the top 10 predicted activated (in red) and the top ten inhibited (in blue) upstream regulators. IPA ranking (1 to 10) identified from the most to the less significant upstream regulator.

Online Table V

Gene Ontology analysis on FOXO targets genes

Gene Ontology Term		Category, Level	Set Size	Candidates contained	*p* -value	*q* -value
GO:0012501	Programmed Cell Death	BP 4	1320	38 (2.9%)	1.25E-13	5.62E-11
GO:0048523	Negative Regulation of Cellular Process	BP 4	2601	51 (2.0%)	8.62E-12	1.94E-09
GO:0071310	Cellular Response to Organic Substance	BP 4	1019	30 (3.0%)	5.02E-11	7.53E-09
GO:0010941	Regulation of Cell Death	BP 4	986	29 (3.0%)	1.17E-10	1.32E-08
GO:0048522	Positive Regulation of Cellular Process	BP 4	2753	49 (1.8%)	8.91E-10	8.02E-08
GO:0042127	Regulation of Cell Proliferation	BP 4	1021	28 (2.8%)	1.29E-09	9.66E-08
GO:0071241	Cellular Response to Inorganic Substance	BP 4	73	9 (12.3%)	3.30E-09	2.12E-07
GO:0010646	Regulation of Cell Communication	BP 4	1971	38 (1.9%)	1.65E-08	9.28E-07
GO:0009893	Positive Regulation of Metabolic Process	BP 4	1817	36 (2.0%)	2.43E-08	1.22E-06
GO:0007517	Muscle Organ Development	BP 4	352	15 (4.3%)	5.19E-08	2.33E-06
GO:0001944	Vasculature Development	BP 4	532	18 (3.4%)	7.25E-08	2.93E-06
GO:0010038	Response to Metal Ion	BP 4	177	11 (6.2%)	7.81E-08	2.93E-06
GO:2000026	Regulation of Multicellular Organismal Development	BP 4	1180	27 (2.3%)	1.10E-07	3.81E-06
GO:0060537	Muscle Tissue Development	BP 4	377	15 (4.0%)	1.32E-07	4.23E-06
GO:0070848	Response to Growth Factor Stimulus	BP 4	331	14 (4.3%)	1.56E-07	4.69E-06
GO:0070997	Neuron Death	BP 4	194	11 (5.7%)	1.99E-07	5.35E-06
GO:0042692	Muscle Cell Differentiation	BP 4	336	14 (4.2%)	2.02E-07	5.35E-06
GO:0009966	Regulation of Signal Transduction	BP 4	1752	33 (1.9%)	3.27E-07	7.41E-06
GO:0072358	Cardiovascular System Development	BP 4	791	21 (2.7%)	3.29E-07	7.41E-06
GO:0072359	Circulatory System Development	BP 4	791	21 (2.7%)	3.29E-07	7.41E-06
GO:0009889	Regulation of Biosynthetic Process	BP 4	3114	47 (1.5%)	3.83E-07	8.20E-06
GO:0060255	Regulation of Macromolecule Metabolic Process	BP 4	3845	53 (1.4%)	9.28E-07	1.90E-05
GO:0048545	Response to Steroid Hormone Stimulus	BP 4	232	11 (4.7%)	1.24E-06	2.43E-05
GO:0036293	Response to Decreased Oxygen Levels	BP 4	189	10 (5.3%)	1.37E-06	2.57E-05
GO:0035556	Intracellular Signal Transduction	BP 4	1710	31 (1.8%)	1.95E-06	3.51E-05
GO:0009892	Negative Regulation of Metabolic Process	BP 4	1382	27 (2.0%)	2.27E-06	3.94E-05
GO:0051094	Positive Regulation of Developmental Process	BP 4	694	18 (2.6%)	3.40E-06	5.67E-05
GO:0014070	Response to Organic Cyclic Compound	BP 4	498	15 (3.0%)	4.00E-06	6.42E-05
GO:0033993	Response to Lipid	BP 4	502	15 (3.0%)	4.30E-06	6.67E-05
GO:0097190	Apoptotic Signaling Pathway	BP 4	442	14 (3.2%)	4.78E-06	7.09E-05
GO:0009743	Response to Carbohydrate Stimulus	BP 4	129	8 (6.2%)	4.93E-06	7.09E-05
GO:0080090	Regulation of Primary Metabolic Process	BP 4	3945	52 (1.3%)	5.04E-06	7.09E-05

Biological Process enriched in FOXO TFs target genes using Gene Ontology.

Online Table VI

Echocardiographic parameters at 4 weeks of age in the experimental groups

	WT	***Lmna*$^{-/-}$**	***Lmna*$^{-/-}$*:AAV9-Gfp***	***Lmna*$^{-/-}$:AAV9-FOXO^{shRNA}**	**ANOVA**
N	18	12	9	16	
M/F	7/11	6/6	3/6	9/7	
Age (days)	28.2±2.1	28.4±1.9	28.5±1.1	29.4±11	0.19
Body weight (g)	14.1±3.7	7.95±1.8***	9.99±1.3 §§	9.7±2.2‡‡‡	<0.0001
HR (bpm)	524±72	514±68	565±66	550±97	0.37
IVST (mm)	0.59±0.049	0.54±0.063	0.59±0.055	0.52±0.044‡‡, ##	0.0004
PWT (mm)	0.60±0.1	0.54±0.06	0.55±0.07	0.48±0.07‡‡	0.0018
LVEDD (mm)	3.27±0.3	2.82±0.47	3.54±0.41§§	3.44±0.61‖‖	0.0021
LVEDDi (mm/g)	0.24±0.05	0.36±0.04***	0.36±0.05†††,§§	0.36±0.05‡‡‡	<0.0001
LVESD (mm)	1.57±0.26	1.86±0.58	2.7±0.63†††,§	2.63±0.86‡‡‡,‖‖	<0.0001
LVESDi (mm/g)	0.244±0.05	0.36±0.04***	0.36±0.05†††	0.36±0.05‡‡‡	<0.0001
FS (%)	52.17±6.64	35.12±8.36***	24.56±9.45§§§	25.31±12.86‡‡‡	<0.0001
LVM (mg)	54.62±12.47	37.81±14.37**	58.48±11.47§§	47.28±12.95	0.0016
LVMi (mg/g)	3.99±0.89	4.67±0.71	5.82±0.68†††,§	4.94±0.88‡‡	<0.0001

Abbreviations: As in Table II

*:$p \leq 0.05$, **: $p \leq 0.01$, ***: $p \leq 0.001$ for *Lmna*$^{-/-}$ *vs* WT.
† $p \leq 0.05$, ††: $p \leq 0.01$, †††: $p \leq 0.001$ for *Lmna*$^{-/-}$:GFP *vs* WT.
‡:$p \leq 0.05$, ‡‡: $p \leq 0.01$, ‡‡‡: $p \leq 0.001$ for *Lmna*$^{-/-}$:FOXO^{shRNA} *vs* WT.

§:$p \leq 0.05$, §§: $p \leq 0.01$, §§§: $p \leq 0.001$ for *Lmna*$^{-/-}$:GFP *vs Lmna*$^{-/-}$.
‖:$p \leq 0.05$, ‖‖: $p \leq 0.01$, ‖‖‖: $p \leq 0.001$ for *Lmna*$^{-/-}$:FOXO^{shRNA} *vs Lmna*$^{-/-}$.

#:$p \leq 0.05$, ##: $p \leq 0.01$, ###: $p \leq 0.001$ for *Lmna*$^{-/-}$:FOXO^{shRNA} *vs Lmna*$^{-/-}$:GFP.

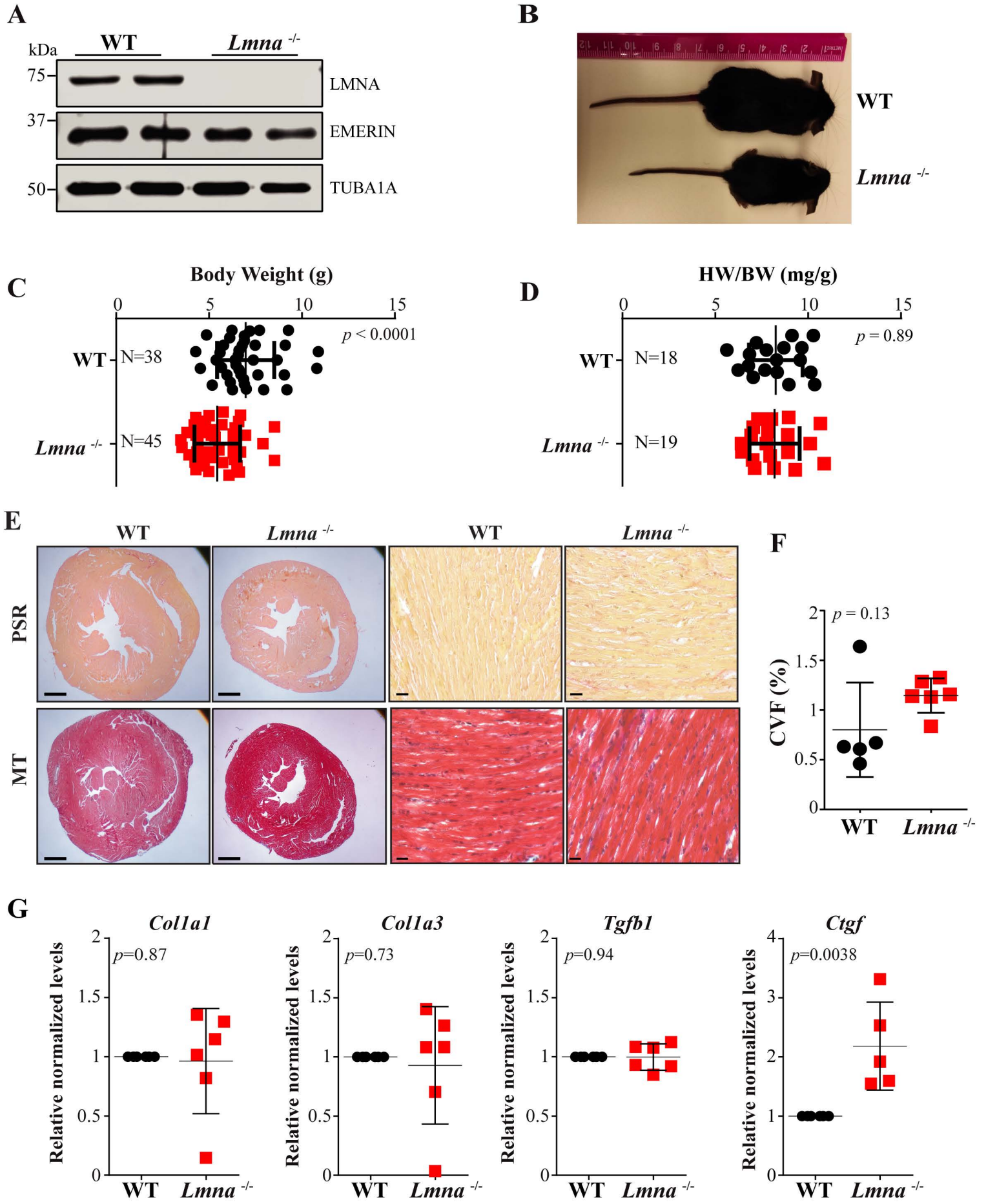

Online Figure I: Phenotype of the *Lmna*$^{-/-}$ mice at 2 weeks of age, the time point used for RNA-Sequencing.
A. Immunoblot showing absence of the LMNA protein in the *Lmna*$^{-/-}$ mice. Emerin and tubulin α1 (TUBA1A) as controls. **B.** Gross morphology **C.** Body weight. **D.** HW/BW ratio. **E.** Representative low and high magnification myocardial sections stained for Picro-Sirius Red (PSR) and Masson's trichrome (MT) showing absence of intrestitial fibrosis. Scale bar is Bar is 200 μm in left panels and 20 μm in right panels **F.** Collagen volume fraction (CVF). **G.** Transcript levels of selected genes invovled in fibrosis: collagen, type Iα1 (*Col1a1*), collagen, type IIIα1 (*Col3a1*), transforming growth factor *β*1 (*Tgfβ1*), and connective tissue growth factor (*Ctgf*), as determined by qRT-PCR.

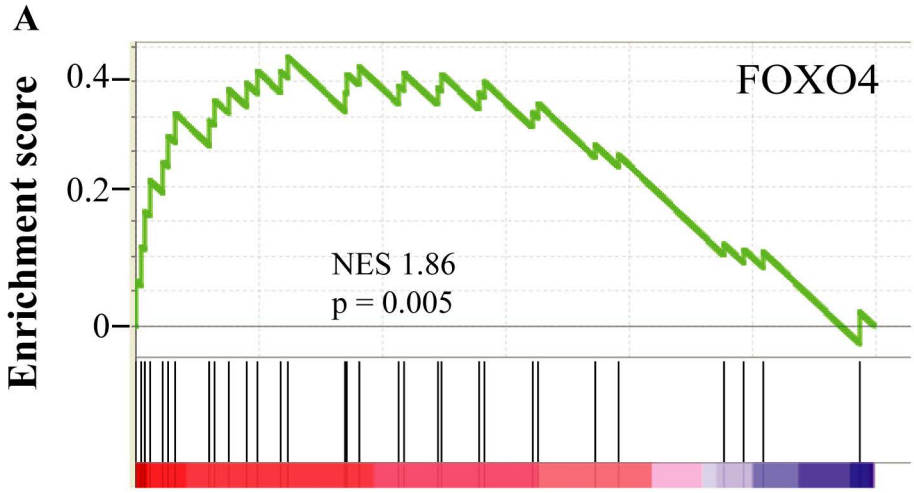

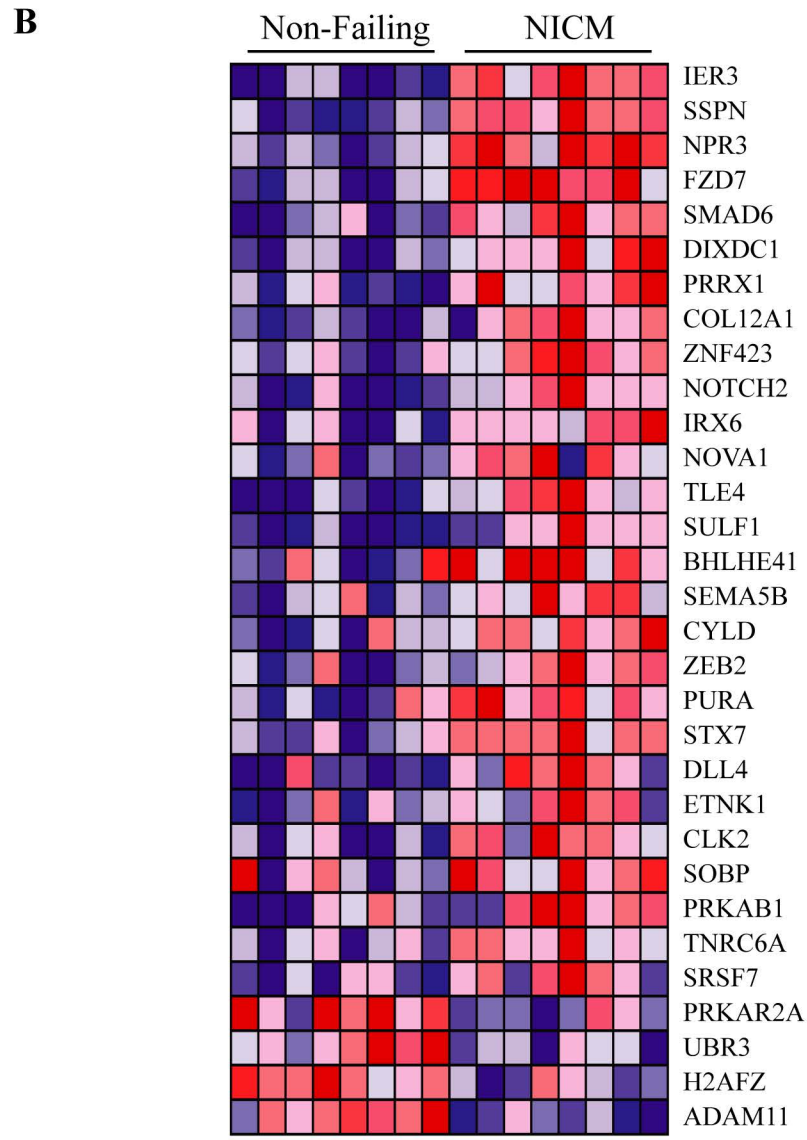

Online Figure II: Differenitally expressed transcripts of FOXO TF tagets in human dilated cardiomyopathy with undefined mutation.

GSEA analysis for transcription factor motif enrichment of Human RNA-seq data (GSE46224) obtained from left ventricular tissues of adult non-failing and non-ischemic cardiomyopathy (NICM) hearts with undefined causal mutations.

A. GSEA enrichment plot of FOXO transcription factors, which were identified by the enrichment of their canonical binding site (TTGTTT_V$FOXO4_01). The motif was among the top 10 enriched TF motifs.

B. Heat map showing FOXO TF target transcripts that indicate activation of FOXO TF in the GSEA analysis.

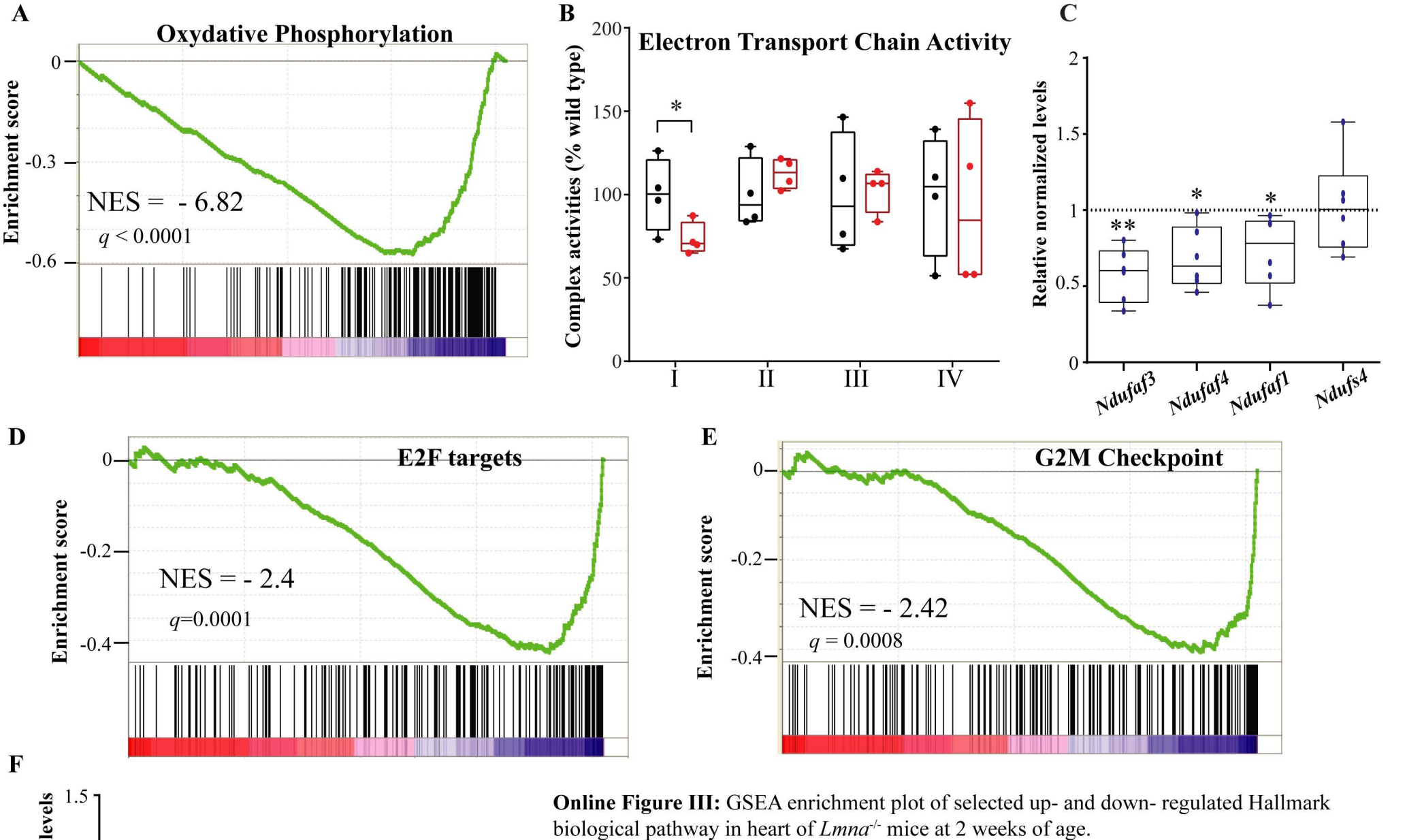

Online Figure III: GSEA enrichment plot of selected up- and down- regulated Hallmark biological pathway in heart of *Lmna*$^{-/-}$ mice at 2 weeks of age.

A. GSEA plot of Oxydative Phosphorylation, showing suppression.

B. Electron transport chain activity of mitochondrial complex I-IV showing reduced activity of complex I.

C. qPCR data showing reduced transcript levels of selected genes involved in Complex I activity.

D . GSEA plot of the cell cycle regulator E2F pathway showing suppression

E. GSEA plot of G2M checkpoint showing significant down-regulation, consistent with suppression of the E2F TF pathways

F. qPCR data showing reduced transcript levels of selected genes involved in cell cycle regulation

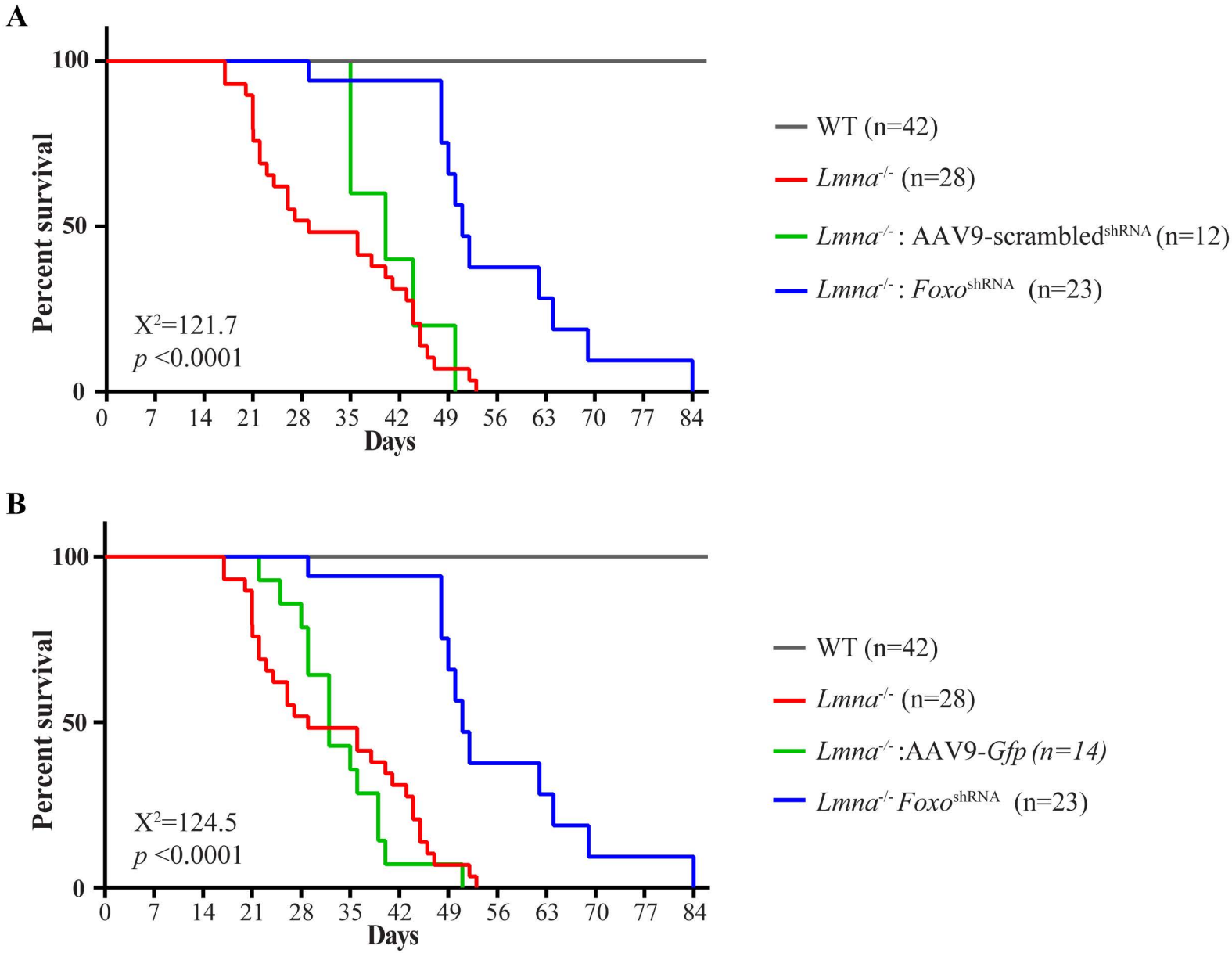

Figure IV: Kaplan-Meier survival plots of wild type (WT), *Lmna*$^{-/-}$ mice (not injected) and *Lmna*$^{-/-}$ mice injected either with a AAV9-scrambled^{shRNA} (Panel A) or AAV9:*Gfp* (Panel B) constructs as two separate controls or with the AAV9-*Foxo*^{shRNA} construct. Survival improved in the AAV9-*Foxo*^{shRNA} in both experiments as compared to control viruses or not injected *Lmna*$^{-/-}$ mice.

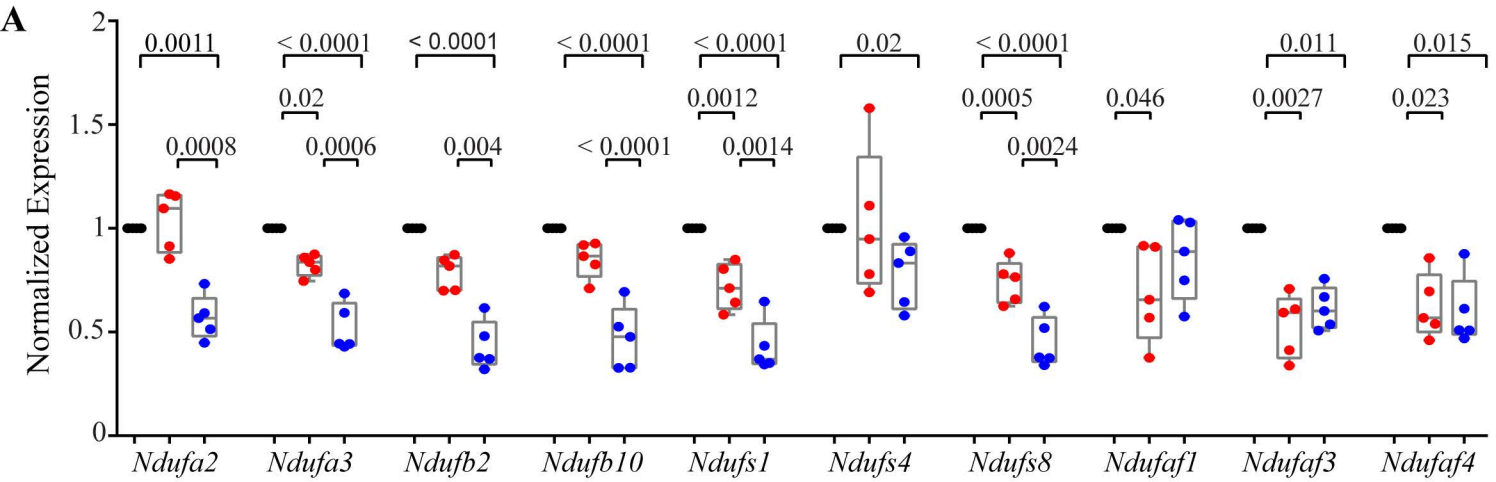

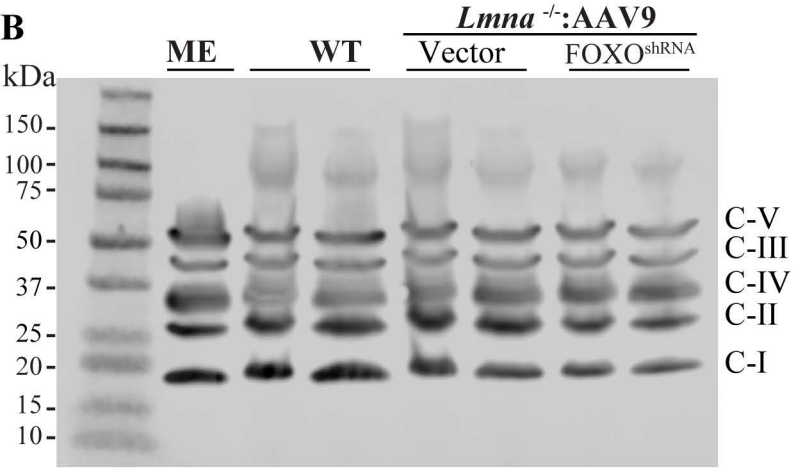

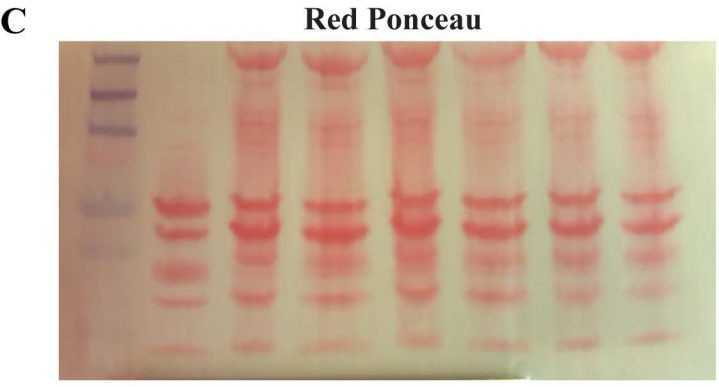

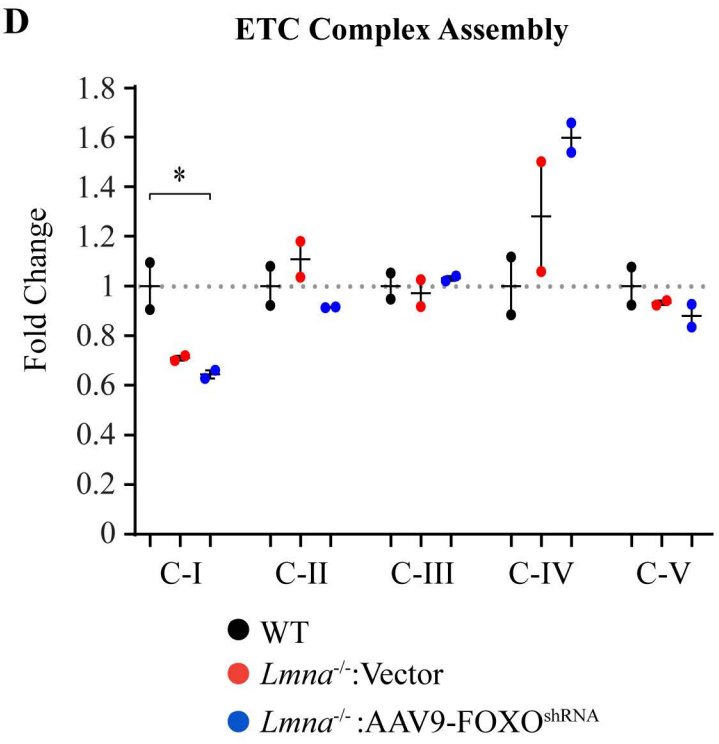

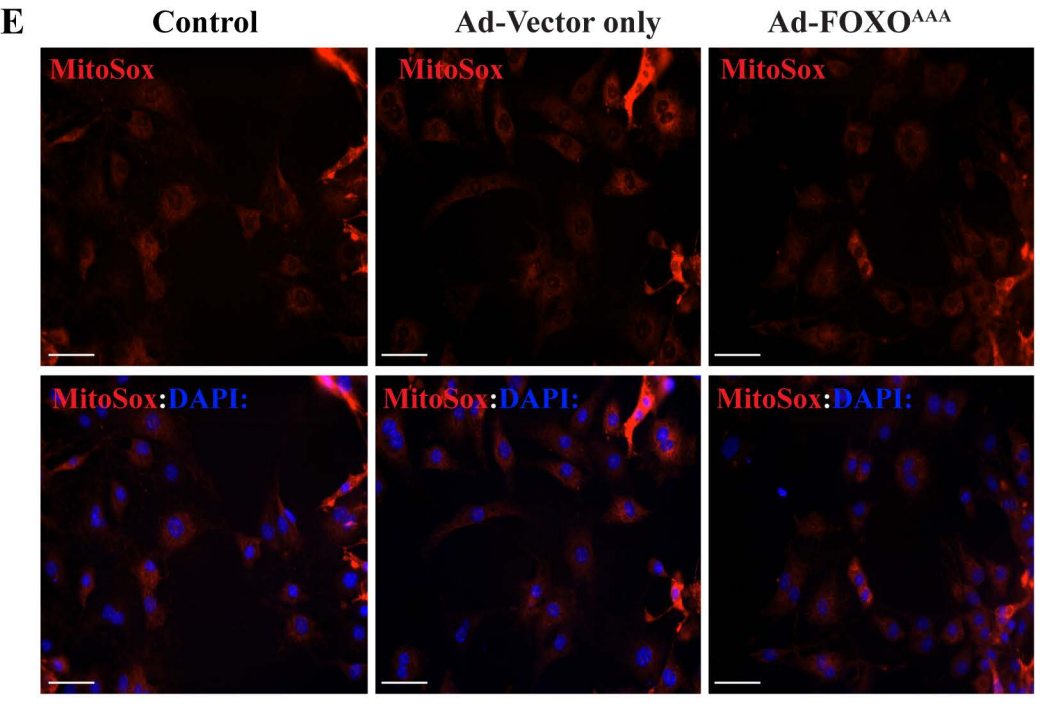

Online Figure V: Assessment of mitochondrial function:
A. Relative transcript levels of genes involved in complex I function and assembly.
B. Western blot showing selective mitochondrial complex proteins reflective of their respective complex assembly
C. Ponceau stained membrane showing equal protein loading
D. Quantitative data of mitochondrial ETC complex proteins
E. MitoSOX assay showing superoxide production in mouse neonatal cardiac myocytes
ME: Rat mitochondrial extract as a positive control
ETC: Electron chain transport

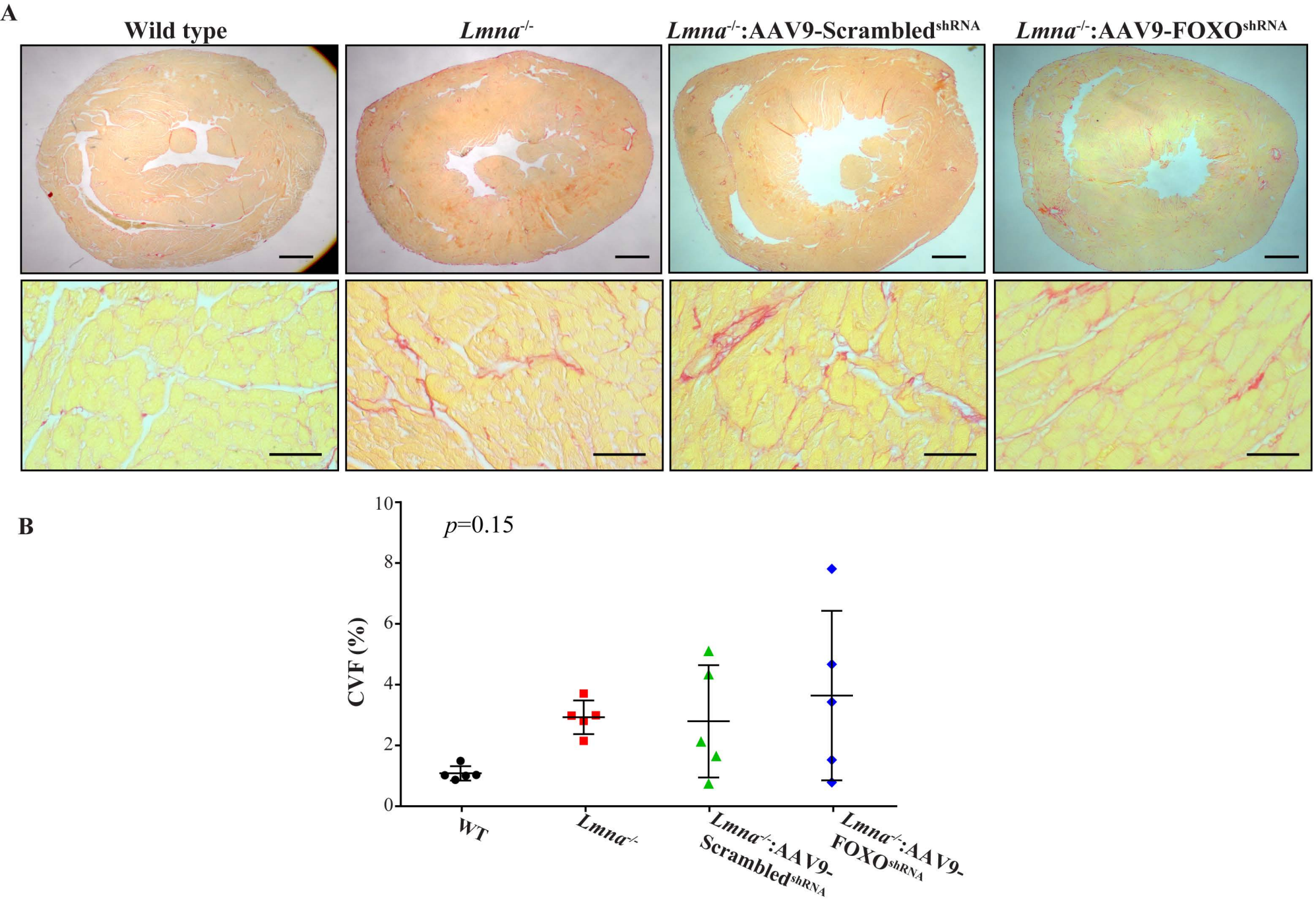

Online Fiigure VI: Interstitial fibrosis in the wild type, *Lmna*$^{-/-}$, *Lmna*$^{-/-}$ treated with AAV9-Scrambled^{shRNA} and *Lmna*$^{-/-}$ treated with AAV9-FOXO^{shRNA} **A.** Low (x2) and high (X40) magnification fields of picro sirius red stained thin myocardial sections in the experimental groups. Scale bar is 200µm and 20µm. **B.** Quantitative collagen volume fraction (CVF) as percent of the myocadium in the experimental groups.

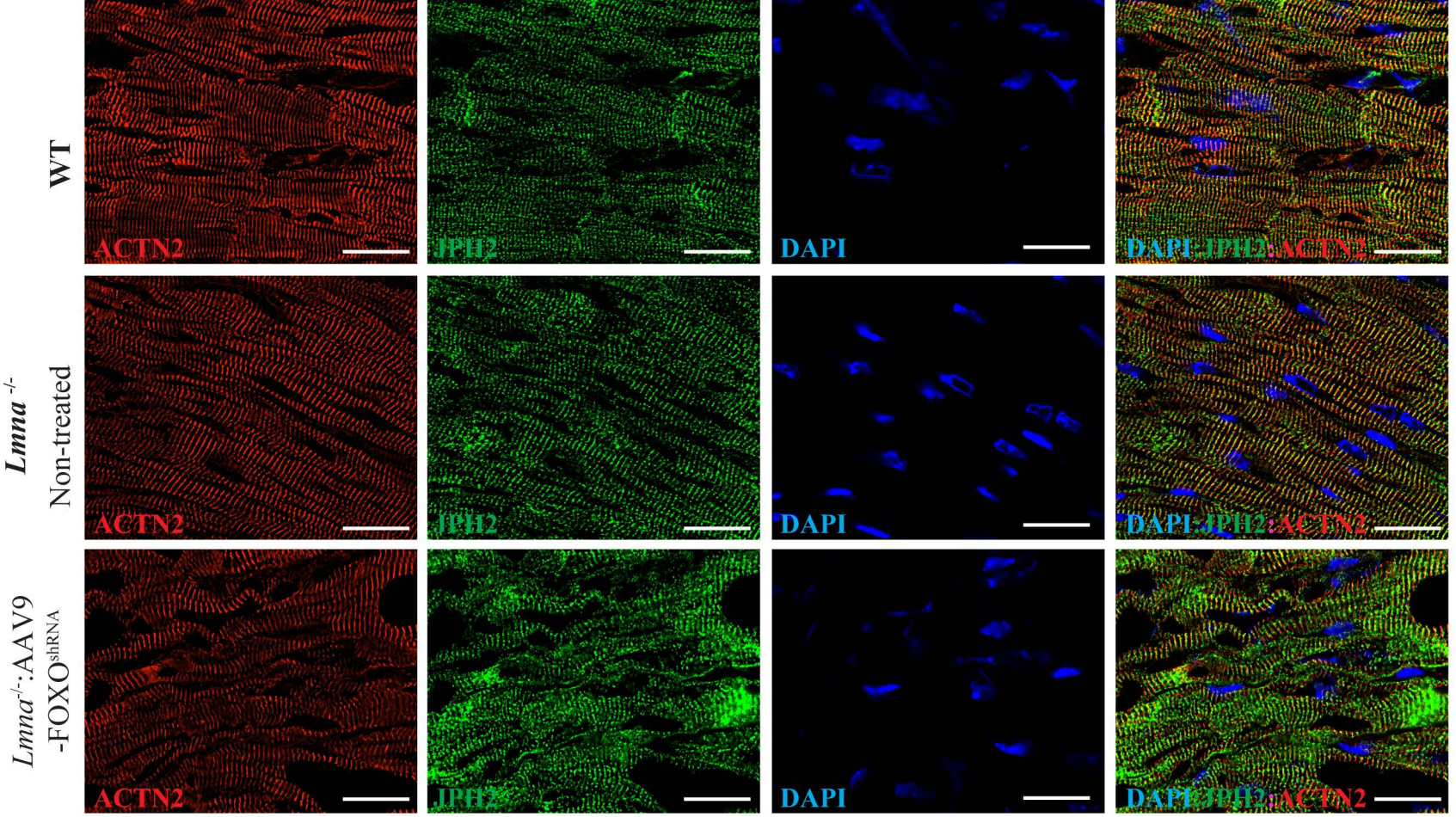

Online Figure VII. Myocardial structure
Immunofluorescence staining of thin myocardial sections for actinin alpha 2 (ACTN2), and junctophilin 2 (JPH2) in wild type (WT), Lmna-/- mice and Lmna$^{-/-}$ mice treated with an AAV9 construct expressing an shRNA against FOXO transcription factors (Lmna$^{-/-}$:AAV9-FOXO^{shRNA})